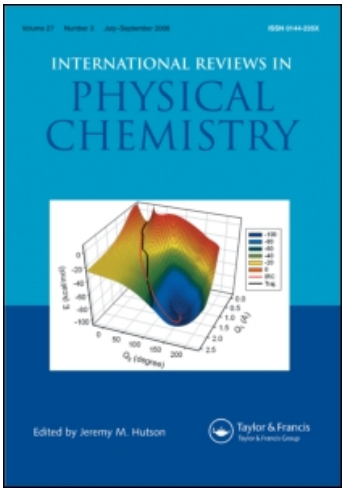

International Reviews in Physical Chemistry
Publication details, including instructions for authors and subscription information:
http://www.informaworld.com/smpp/title~content=t713724383

Spectroscopic studies of cold, gas-phase biomolecular ions

Thomas R. Rizzo[a]; Jaime A. Stearns[a]; Oleg V. Boyarkin[a]
[a] Laboratoire de Chimie Physique Moléculaire, École Polytechnique Fédérale de Lausanne, Lausanne, CH-1015, Switzerland

To cite this Article Rizzo, Thomas R. , Stearns, Jaime A. and Boyarkin, Oleg V.(2009) 'Spectroscopic studies of cold, gas-phase biomolecular ions', International Reviews in Physical Chemistry, 28: 3, 481 — 515
To link to this Article: DOI: 10.1080/01442350903069931
URL: http://dx.doi.org/10.1080/01442350903069931

International Reviews in Physical Chemistry
Vol. 28, No. 3, July–September 2009, 481–515

Taylor & Francis
Taylor & Francis Group

Spectroscopic studies of cold, gas-phase biomolecular ions

Thomas R. Rizzo*, Jaime A. Stearns and Oleg V. Boyarkin

Laboratoire de Chimie Physique Moléculaire, École Polytechnique Fédérale de Lausanne, CH-1015 Lausanne, Switzerland

(*Received 13 April 2009; final version received 20 May 2009*)

While the marriage of mass spectrometry and laser spectroscopy is not new, developments over the last few years in this relationship have opened up new horizons for the spectroscopic study of biological molecules. The combination of electrospray ionisation for producing large biological molecules in the gas phase together with cooled ion traps and multiple-resonance laser schemes are allowing spectroscopic investigation of individual conformations of peptides with more than a dozen amino acids. Highly resolved infrared spectra of single conformations of such species provide important benchmarks for testing the accuracy of theoretical calculations. This review presents a number of techniques employed in our laboratory and in others for measuring the spectroscopy of cold, gas-phase protonated peptides. We show examples that demonstrate the power of these techniques and evaluate their extension to still larger biological molecules.

Keywords: gas-phase biological molecules; cooled ion traps; electrospray; infrared spectroscopy

Contents

*Corresponding author. Email: thomas.rizzo@epfl.ch

ISSN 0144–235X print/ISSN 1366–591X online

DOI: 10.1080/01442350903069931
http://www.informaworld.com

1. Introduction

Because the functions of biological molecules are intimately connected to their three-dimensional structure, an enormous amount of effort is expended to determine the latter with the hope of understanding, and perhaps intervening in, the former. While biomolecular structure is determined primarily by x-ray crystallography and NMR, theory is playing an increasingly important role. As available computational power continues its exponential rise, increasingly large molecules become amenable to theoretical treatment. In addition to its potential predictive power, an accurate theoretical description of biological molecules allows one to dissect and analyse the counterbalancing forces that control their structure as well as to examine the properties of individual stable conformers. To make sure that theoretical treatments properly describe the underlying physics and are capable of reliably predicting structures, comparison with benchmark experiments is essential. Perhaps the most rigorous test is to compare theory and experiment on isolated biological molecules, free from the complicating effects of solvent.

In the mid-1980s molecular spectroscopists began to remove biological molecules from their natural environment to interrogate them in the cold, isolated environment of supersonic molecular beams [1–9]. Early experiments used electronic spectroscopy to investigate the amino acid tryptophan with the goal of determining the number of stable conformations that it could adopt *in vacuo* [1–4]. This was driven by observations that the fluorescence decay rate of tryptophan in solution, which is used as a monitor of protein folding, is non-exponential [10–12], and one of the models to explain these observations postulated the existence of different 'conformers' having different fluorescence quenching rates[12]. Electronic spectra of isolated tryptophan did indeed identify a number of stable conformations[4], although at the time theoretical methods were not able to make reasonable predictions for these structures. Today the conformations of isolated amino acids can be easily and reliably calculated.

The earliest experiments on isolated amino acids [1–4] and their derivatives [8,13,14] used simple heating to put them in the gas phase. With the advent of laser desorption techniques, larger, more complex molecules could be volatilised without decomposition [5–7, 15], and this helped ignite an explosion in spectroscopic studies of neutral peptides with up to 15 amino acid residues [5,6,9, 16–29]. The increasing complexity of these molecules require more sophisticated spectroscopic techniques to extract structural information, and this has been achieved by employing IR–UV [18–21,23,24,26, 30–40], UV–UV [30,33,36,41] and even IR–IR–UV multiple-resonance methods [42] together with cooling in supersonic expansions.

Still larger biological molecules become increasingly difficult to produce in the gas phase *via* thermal techniques without decomposition. The advent of MALDI [43,44] and electrospray [45,46] in mass spectrometry has allowed intact biological molecules of virtually any size to be put into the gas phase in the form of closed-shell molecular ions and opened up new avenues of investigation. Bowers and co-workers used these techniques together with ion mobility to characterise the average cross section of such species [47,48]. Wang and co-workers measured photoelectron spectra of multiply-charged, non-biological anions generated by electrospray [49], and Parks and co-workers observed fluorescence from cytochrome C in an electrospray plume [50] and later from small proteins in a quadrupole ion trap [51]. However it was Andersen *et al*. [52,53] who first used absorption/action spectra to characterise closed-shell biomolecular ions produced by electrospray. These groundbreaking experiments measured electronic absorption spectra of green fluorescent protein chromophore in an electrostatic ion storage ring by detecting the neutral products subsequent to either photodetachment (in the case of anions) or photofragmentation (in the case of cations). The spectra they obtained exhibited only broad structure, although this is likely due to the warm internal temperatures of the ions in the storage ring. At about the same time, McLafferty *et al*. [54,55] demonstrated that one could do infrared multiphoton dissociation (IRMPD) of electrosprayed peptides and proteins in a Fourier transform ion-cyclotron resonance (FT-ICR) mass spectrometer using an optical parametric oscillator (OPO) operating in the light-atom stretch region. Tuning the frequency of their IR OPO produced photofragment excitation spectra that reflect the infrared absorption of OH and NH stretch vibrations. Even though the ions in their trap were at room temperature, the observed bands were about $30\,cm^{-1}$ wide, which is sufficiently narrow to distinguish many light atom stretch bands. Von Helden *et al*. [56] extended IRMPD spectroscopy into the amide I and II regions of the infrared using a free electron laser to measure infrared spectra of potassiated cytochrome C ions formed by electrospray, where detection of infrared absorption was monitored by the loss of the potassium adduct. Although the individual bands in these spectra were rather broad ($30–50\,cm^{-1}$), the overall vibrational pattern in this region suggests a large degree of α-helical content. Shortly thereafter, Kamariotis *et al*. [57] measured infrared spectra of solvated amino acid ions to look for evidence of zwitterion formation by detecting solvent loss subsequent to IR absorption. These spectra were used to test the claim that after adding 3–4 water molecules a cationised amino acid exists in a salt-bridge arrangement with the amino acid in a zwitterionic form [58].

While all these studies broke new ground in providing spectroscopic data to help characterise the conformational properties of closed-shell biomolecular ions, the spectral complexity was substantially greater and the resolution correspondingly lower than studies of neutrals cooled in supersonic expansions. Simons *et al*. [59–61] developed a photochemical method for producing protonated biological molecules in a supersonic expansion, and while perhaps not the most widely applicable, this approach demonstrated that the spectra of closed-shell ions are inherently no more complex than their corresponding neutrals. As the size and spectral complexity of the molecules increase, cooling the molecules is simply necessary to facilitate spectroscopic analysis.

In a major step toward spectroscopic studies of cold, biomolecular ions, Weinkauf *et al*. [62] measured the electronic excitation spectrum of protonated tryptophan produced by electrospray and stored in a liquid-nitrogen-cooled quadrupole ion trap. While the

electronic spectrum they obtained showed some structure, the spectral features were orders of magnitude broader than molecules cooled in a supersonic expansion, leading one to question the cooling efficiency in their trap. It was later discovered that the spectrum of protonated tryptophan is inherently broad due to fast excited state dynamics [63]. Nevertheless, Weinkauf's [62] experiments served as a major stimulus to study electrosprayed ions in cold traps.

This present article reviews the work currently being done in the authors' laboratory combining electrospray ionisation for producing gas-phase biomolecules together with collisional cooling in a cold 22-pole ion trap and IR–UV double-resonance techniques to simplify the spectra. The primary goals of this work have been to understand the intrinsic properties of biological molecules and provide critical benchmark tests of theory, and for this we look at bare, isolated molecules in the gas phase. While as a test of theory, the spectroscopy of gas-phase biomolecules has relevance completely apart from their condensed phase analogs, the closed-shell molecular ions produced by electrospray are the same species found in solution, where most biomolecules carry a net charge. Moreover, by examining partially solvated molecules in the gas phase, we can begin to understand the role of solvent on those properties.

2. Experimental and computational approach

2.1. *Overview*

We perform our experiments in a home-built ion-trap mass spectrometer, shown schematically in Figure 1. Rather than give a detailed description of this apparatus, which can be found in recent publications [64–70], we provide a brief overview of the experimental approach followed by an explanation of key aspects of the experimental design.

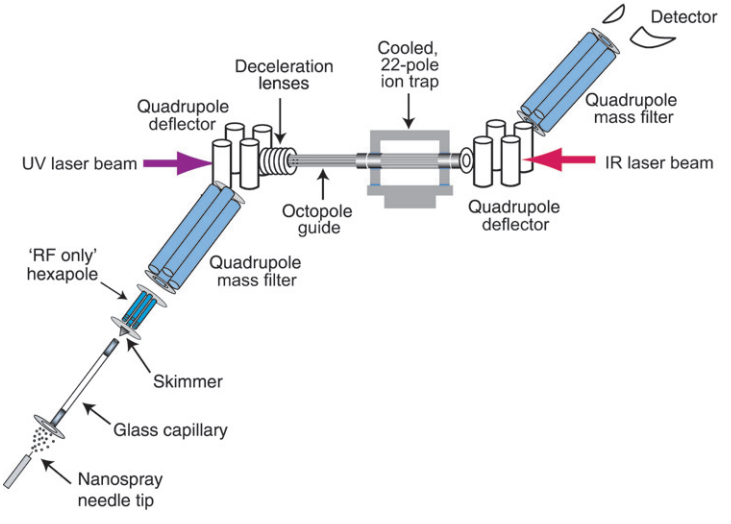

Figure 1. [Colour online] Schematic of tandem mass spectrometer with a cooled, 22-pole ion trap. Adapted with permission from [86]. Copyright 2006 American Chemical Society.

We use a nanospray source to produce the protonated peptides from an acidified water/methanol solution directly into the atmosphere, where they are drawn into vacuum by a metal-coated glass capillary. The expansion that occurs at the exit of the capillary passes through a 1 mm diameter skimmer and into a hexapole ion trap, where the ions are collected for ~50 ms. Once released from the hexapole, the resulting ion packet passes through a quadrupole mass filter to select those of a particular m/z. The transmitted ions are then turned 90° by a static quadrupole deflector, decelerated by a series of lenses and guided by an octopole ion guide into a 22-pole ion trap, which is cooled to ~6 K by a closed-cycle refrigerator. Before the ion packet arrives in the trap, we inject a pulse of helium, giving it sufficient time to equilibrate to the temperature of the trap housing. The ions collide with the cold helium and fall in to the effective potential well of the trap. We give the ions approximately 10 ms to cool and then wait an additional 30 ms to pump out the helium before we interrogate them spectroscopically.

We pass a UV laser pulse from a frequency-doubled dye laser down the axis of the 22-pole ion trap, promoting the molecules to an excited electronic state from which some fraction of them dissociate. We then release both the parent and fragment ions from the trap, turn them 90° in a second static quadrupole and pass them through an analysing quadrupole to select an m/z of either a particular fragment or of the parent ions. The transmitted ions are then detected by a channeltron electron multiplier. An electronic spectrum is obtained by recording the ion signal of a particular fragment as a function of the frequency of the UV laser. As is described more fully below, we measure infrared spectra of the trapped biomolecular ions using IR–UV double resonance.

The trapping cycle of the ions is repeated at 20 Hz. We switch the analysing quadrupole to transmit either the fragment or the parent on alternate trapping cycles and use the parent signal from one shot to normalise the fragment signal from the subsequent one, which removes long-term fluctuations in the nanospray source.

2.2. *Ion generation*

Putting biological molecules into the gas-phase *via* electrospray has many advantages for spectroscopic studies. Because they are produced near room temperature and at atmospheric pressure, there is essentially no fragmentation. There seems to be no limit to the size of molecules that can be produced – those ranging from individual amino acids to entire viruses [71–73] have been successfully injected into mass spectrometers by electrospray. Because we are working with charged biomolecules as opposed to neutrals, we can select their mass and control their trajectories, allowing us to guide and/or trap them. Electrospray generates closed-shell molecular ions, either protonated or deprotonated, which is precisely what is found in solution. The disadvantage of studying biomolecular ions is the relatively low number density, which is a function both of the electrospray process itself as well as space charge effects inside the ion trap.

2.3. *Cooling and trapping*

The linear, 22-pole ion trap is the key element of our experimental apparatus, allowing us to store the molecules and cool them through collisions with cold helium. Gerlich *et al.* [74–76] pioneered the use of cold, RF ion traps and applied them principally to study the

spectroscopy and chemical reaction kinetics of small ions of astrophysical importance. There is nothing particularly special about the choice of 22 poles – it is simply important to have a sufficiently large number of them so that the effective radial potential is flat for a substantial fraction of the trap diameter [76]. As the ions ride up the radial potential wall when they approach the poles, they undergo oscillatory motion driven by the RF field, and collisions with helium at this point could warm the ions as opposed to cooling them. Thus a flat radial potential with steeper walls should facilitate collisional cooling of ions, since in this case the oscillatory motion and hence warming collisions, will be limited to a small fraction of the trap volume. The drawbacks to using a larger number of poles is that the ions spread over a larger volume resulting in a lower ion density on the axis of the trap, and optical access to the trapped ions in the radial direction is limited.

2.4. *Spectroscopic interrogation*

We typically inject 10,000 ions into the 22-pole trap, which has an active volume of ~5 cm. Given the ion density of $\sim 2 \times 10^3\,\mathrm{cm}^{-3}$, it is clear that any kind of direct absorption spectroscopy would be difficult if not impossible. Moreover, this ion density is at the limit of what can be detected by laser-induced fluorescence (LIF), a problem that is compounded by the unfavourable geometry of the 22-pole ion trap for photon detection. We thus need a more sensitive means of spectroscopic detection, and for this we use photofragmentation.

After UV excitation of an aromatic chromophore in a protonated peptide, some fraction of the ions will fragment, since quantum yields for fluorescence are rarely unity. This can occur either following internal conversion to highly excited vibrational levels of the ground electronic state or by crossing to other electronic states that are dissociative in some coordinate. We thus use mass-resolved detection of photofragments as a sensitive spectroscopic tool. As shown schematically in Figure 2a, we measure electronic spectra of the cold ions in the trap by detecting a particular charged photofragment as a function of the UV wavelength.

Our ultimate goal is to measure infrared spectra of biomolecular ions, since such spectra can provide information on the conformation of the molecule. Using an IR–UV double-resonance scheme, illustrated schematically in Figure 2b, we can measure an IR spectrum of individual conformers of the trapped ions. To do this, we fire an infrared pulse from an OPO 200 ns before the UV pulse, depleting the ground state population each time the infrared frequency coincides with a vibrational transition of the parent molecule. The IR transition is then detected as a dip in the UV photofragmentation signal as the IR frequency is scanned through a vibrational band. For this approach to work, the molecules promoted to a vibrationally excited state must not absorb a UV laser photon of the same frequency as that of the ground state and produce fragments, or if they do, it must be with reduced efficiency. Because the IR-excited molecules will be internally warm, we observe their UV absorption spectrum is substantially broadened and the peak absorption at the UV wavelength is greatly reduced, leading to a dip in the IR spectrum.

While this double-resonance approach imposes the requirement that the molecule of interest have a UV chromophore, it has the great advantage that the UV spectrum can be used to select a particular conformer, since different conformers often have slightly different UV spectra that can be resolved if the molecules are internally cold. Thus, the IR

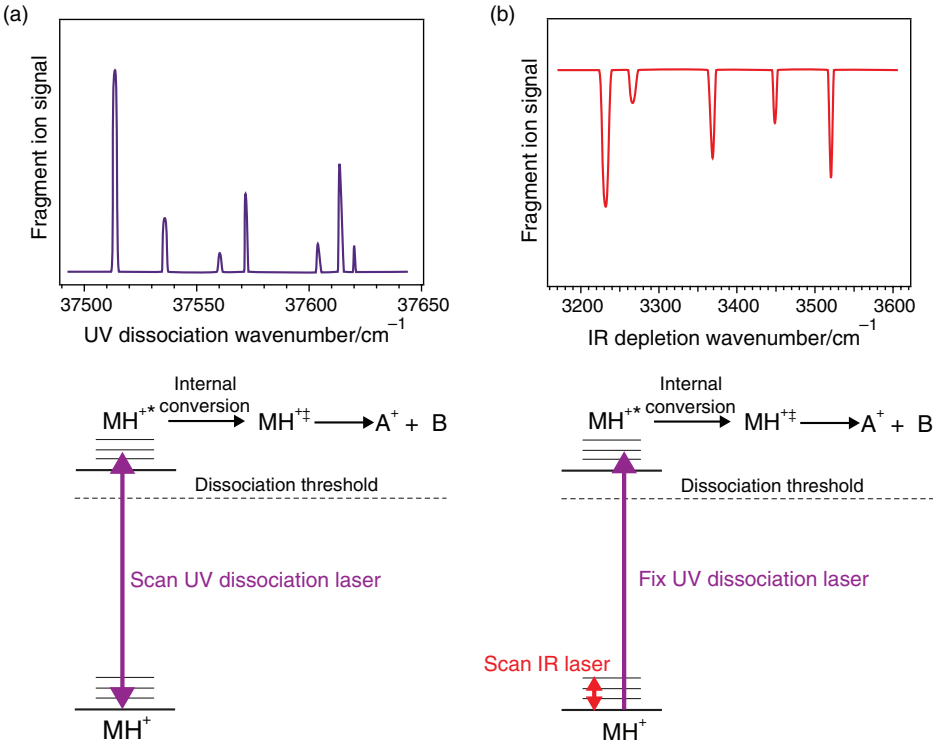

Figure 2. [Colour online] Spectroscopic schemes applied to cold biomolecular ions for measuring (a) electronic spectra of cold biomolecular ions *via* photofragment detection and (b) conformation-specific infrared spectra by detecting the depletion of the UV-induced photofragment signal.

spectra that we obtain are those of single conformations of molecule of interest, which greatly facilitates the assignment of the spectra as well as their comparison with the predictions of theory.

There is one potential limitation to photofragment-based spectroscopic approaches using UV excitation. In the case where fast internal conversion after UV excitation creates a highly vibrationally excited molecule in the ground electronic state, one expects that the unimolecular dissociation rate will decrease with the increasing size of molecule to the point that it may become comparable to the rate of infrared radiation or collisional deactivation with residual helium in the trap, both of which will compete with dissociation. Thus, we expect that spectroscopic detection by single-photon photofragmentation may become more difficult with increasing molecular size, although it is not clear where this limit will be. In Section 6, we will give an example of how we are overcoming this limitation.

2.5. *Computational methods*

Our computational approach begins with a conformational search using the AMBER force field [77] within the Macromodel package [78]. The procedure generates 50,000

structures in the initial search but retains only those unique conformations under 50 kJ/mol relative energy. For molecules with one or two amino acids, we re-optimise all of the structures found with Macromodel using Gaussian 03 [79] at the B3LYP/6-31++G** level of theory [80,81] and carry out harmonic frequency calculations at the same level. Because more than one thousand conformations may be found in the initial search, we first calculate single-point energies of all the structures using Gaussian at the B3LYP/6-31G** level of theory, and use these energies to decide which structures merit full optimisations and frequency calculations using B3LYP/6-31++G**. In addition, all of the conformations are classified according to the major degrees of freedom (number and type of hydrogen bonds, aromatic ring orientation, etc.), and representative structures of each class are also optimised. The energies we report are zero-point corrected, and harmonic frequencies are scaled by 0.954 for amino acids and 0.952 for helical peptides.

3. Spectroscopy of protonated aromatic amino acids

The three aromatic amino acids, tryptophan, tyrosine and phenylalanine, are naturally occurring candidates for probe chromophores, and it is important to understand their spectroscopy and photophysics before using them in more complex molecules. Extensive work has been done on these aromatic amino acids in their neutral form [2,3,31,34, 82–84], but as we are investigating closed-shell ions, one must understand the effect of the charge on the photophysics. At the same time, protonated amino acids are relatively simple systems with which to determine the degree of cooling, and hence residual thermal inhomogeneous broadening, in our cold ion trap. Finally, spectroscopic studies of protonated amino acids can be used to investigate whether IR–UV double resonance can be combined with photofragment-based detection techniques.

The amino acid tryptophan has clearly been the chromophore of choice for spectroscopic studies of peptides and proteins in solution since it has a strong UV absorption and relatively high fluorescence quantum yield. Much of the gas-phase work on neutral amino acids and peptides have also focussed on tryptophan as a chromophore in an effort to better understand its behaviour in solution – in particular its non-exponential fluorescence decay [10–12]. Despite its wide use, it is not obvious that tryptophan would be the chromophore of choice for the spectroscopic approach taken here. The requirements for a good probe chromophore for photofragmentation-based techniques represent a balance between competing factors. On the one hand, one needs non-radiative processes to occur in the excited electronic state leading to fragmentation, allowing us to detect the absorption of radiation *via* the appearance of fragments. Having a high fluorescence quantum yield means that the fraction of molecules in the electronically excited state that fragment will be correspondingly lower and, in this sense, it might be an advantage to use phenylalanine, with the lowest fluorescence quantum yield, even though it has a lower oscillator strength [85]. On the other hand, if the non-radiative processes are too fast, this will tend to broaden the electronic spectrum and inhibit our ability to resolve individual conformations. Our first goal, then, was to examine the electronic spectra of the protonated amino acids tryptophan, tyrosine and phenylalanine. Given the extensive work done on neutral, gas-phase tryptophan [1–4], we began our studies by examining protonated tryptophan in our cold ion trap.

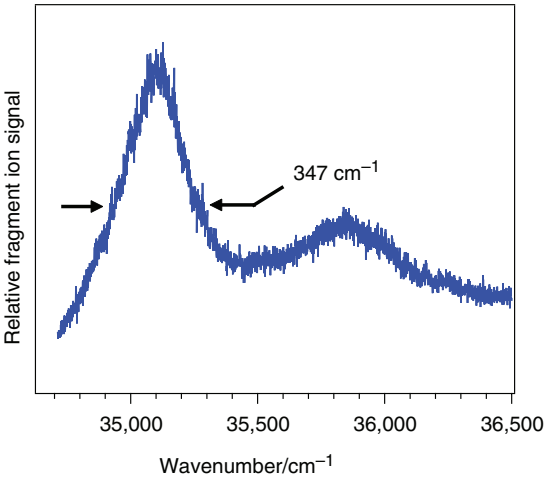

Figure 3. [Colour online] Electronic photofragment excitation spectrum of cold $TrpH^+$ obtained by collecting the fragment ions at m/z 188 as a function of the UV laser wavenumber. Adapted with permission from [86]. Copyright 2006 American Chemical Society.

As in all the aromatic amino acids, protonation of the isolated molecule is expected to occur on the amino group, forming an ammonium (NH_3^+) on the backbone. This is supported by relatively high level calculations [62] and as demonstrated below, is consistent with the spectrum, which is little shifted from the neutral molecule. One would expect protonation on the aromatic ring to cause a substantial shift of the electronic band origin.

Figure 3 shows the photofragment excitation spectrum of $TrpH^+$ in our cold ion trap obtained by collecting the fragment ions at m/z 188 (which corresponds to loss of NH_3) as a function of the wavenumber of the UV laser [86]. As a first test of our new spectroscopic approach, these results were at first rather disappointing. While the broad, primary peak in the spectrum is close to that of the neutral molecule, confirming that protonation does not occur on the indole ring, its breadth suggested that the cooling in the ion trap might not be complete. The spectrum is slightly narrower than that measured by Weinkauf in a quadrupole ion trap cooled to liquid nitrogen temperature [62] as well as that measured by Talbot *et al.* [87] at room temperature, but is far broader than the electronic spectrum of the neutral molecule measured in a supersonic expansion [3]. This initially caused us to question the vibrational temperature of the ions in our 22-pole ion trap and led us to perform a number of diagnostics to verify the degree of cooling. The observation that we could form clusters of protonated amino acids with one or two helium atoms in the trap [68] suggested that the internal temperatures should be on the order of 15 K, assuming the binding energy of helium to a protonated amino acid is similar that that of $NH_4^+ \bullet He$ [88].

A series of papers by Kang *et al.* [63, 89–91] helped provide insight into the reasons for the broad $TrpH^+$ spectrum. The authors used femtosecond laser pulses at 266 nm to excite protonated tryptophan and tyrosine generated by electrospray but not cooled, and then probed the population of the excited state using an 800 nm photon, which can excite the molecule to higher states and change the fragmentation pattern. Their results reveal drastically different excited-state lifetimes for protonated tryptophan and tyrosine.

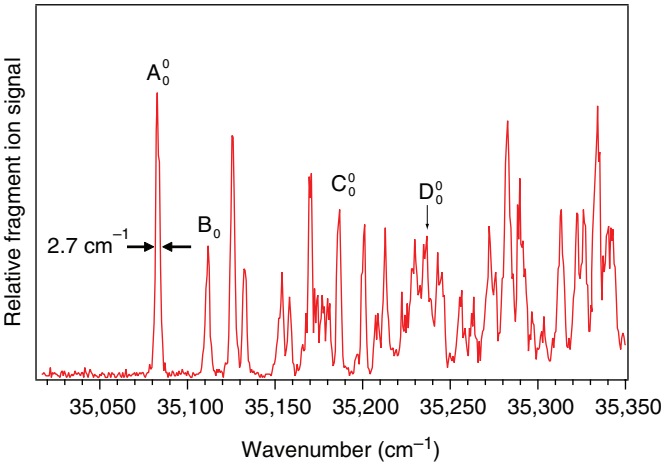

Figure 4. [Colour online] Electronic photofragment excitation spectrum of cold $TyrH^+$ recorded by detecting the fragment at m/z 136. The labels A_0^0–D_0^0 indicate the electronic band origins of four distinct conformers.Adapted with permission from [86]. Copyright 2006 American Chemical Society.

The decay of the π–π^* state in $TrpH^+$ exhibits a rapid drop on a timescale of 380 fs followed by a more complicated behaviour at later times. In contrast, protonated tyrosine exhibits a simple exponential decay of 22 ps. The observation of fast excited state decay in protonated tryptophan suggested that the broad spectrum that we observed may not be the result of incomplete cooling in the ion trap but could be inherently limited by the short lifetime of the excited state. While the overall width of the main feature of $TrpH^+$ (347 cm^{-1}) would imply a much shorter lifetime than that measured by Kang *et al.* [63], it is likely that the spectrum contains contributions from a few stable conformers that may exhibit low frequency vibrational progressions as in the case of the neutral molecule [3]. If each spectral feature were broadened by 13 cm^{-1}, as implied by the 380 fs lifetime measured by Kang *et al.* [63], it could give rise to a broad feature with an overall width on the order of what we observe. Moreover, one should note that the lifetimes determined by Kang *et al.* are upper limits – they cannot rule out even faster excited-state decay. Thus, our ability to form weakly bound helium clusters [68], together with the time-resolved data of Kang *et al.* [63], suggests that the broad feature in the electronic spectrum of $TrpH^+$ is not the result of incomplete cooling but results in large measure from lifetime broadening. If this were the case, then one would expect that spectral features of the other protonated amino acids should be significantly narrower than that of $TrpH^+$.

Figures 4 and 5 show electronic spectra of $TyrH^+$ and $PheH^+$ cooled in our 22-pole ion trap [68], both of which exhibit resolved vibronic features that reflect a significantly longer lifetime than that of protonated tryptophan, consistent with the time-resolved work of Kang *et al.* [63]. These well-resolved spectra can be used as a diagnostic for the internal temperatures of the molecules in our ion trap, demonstrated here for the case of $PheH^+$. As will be shown below, the two most prominent features in the spectrum, which occur at 37,530 cm^{-1} and 37,541 cm^{-1}, correspond to the electronic band origins of two stable conformations of the molecule, and we label these band origins A_0^0 and B_0^0 respectively. The inset of Figure 5 shows a blow-up of the region of the spectrum to the red of these

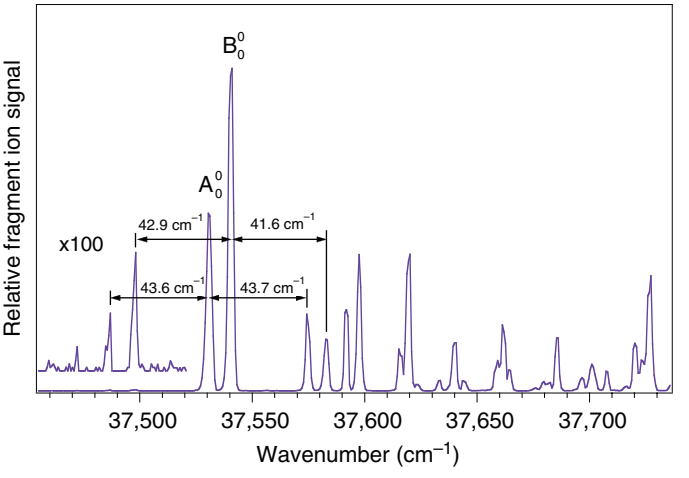

Figure 5. [Colour online] Electronic photofragment excitation spectrum of cold $PheH^+$ recorded by detecting the fragment at m/z 74. The labels A_0^0 and B_0^0 indicate the electronic band origins of two distinct conformers. To the low energy side of these band origins, a blow up of the spectrum shows two low frequency hot bands that help determine the vibrational temperature.

band origins where one would expect hot-bands of low-frequency vibrational modes to occur. One can see two features separated from A_0^0 and B_0^0 by approximately $-43\,cm^{-1}$, which is almost identical to the spacing of the first two small peaks to the high frequency side of the band origins. This suggests that protonated phenylalanine has a low frequency mode of $\sim 43\,cm^{-1}$ in both the ground and excited electronic state. The intensity of the hot bands relative to the band origins gives us an estimate of the vibrational temperature of the molecule, although this requires us to assume a particular oscillator strength for the hot-band transitions. If we assume that the band strength of the hot-bands, X_1^0, is similar to that of its corresponding vibronic band X_0^1, we arrive at a vibrational temperature between 11 and 16 K. This is consistent with the rotational temperature determined from a rough simulation of the band contours. While this might not seem particularly cold, at these internal temperatures the populations of even the lowest frequency vibrational modes do not contribute to spectral congestion in a significant way.

With well-resolved electronic spectra such as those of Figures 4 and 5, we can use IR–UV double resonance to further identify features corresponding to different stable conformations of the parent molecule by measuring an IR spectrum of each conformer. Figure 6 shows IR–UV double-resonance spectra of $PheH^+$ with the UV laser set on one of the two band origins, A_0^0 or B_0^0, in Figure 5. It is evident that these IR spectra are different, confirming that the two features in the electronic spectrum correspond to different stable conformations of the molecule. Even before measuring an IR spectrum, the electronic spectrum of $PheH^+$ suggests the presence of at least two stable conformers. The observation of two strong features near the band origin spaced by $10.6\,cm^{-1}$ without a further progression of peaks at roughly the same spacing suggests that these two features are not members of a Franck–Condon progression, since by their very nature such progressions rarely terminate abruptly. Calculated spectra and the corresponding structures for the two lowest-energy conformers of protonated phenylalanine are also

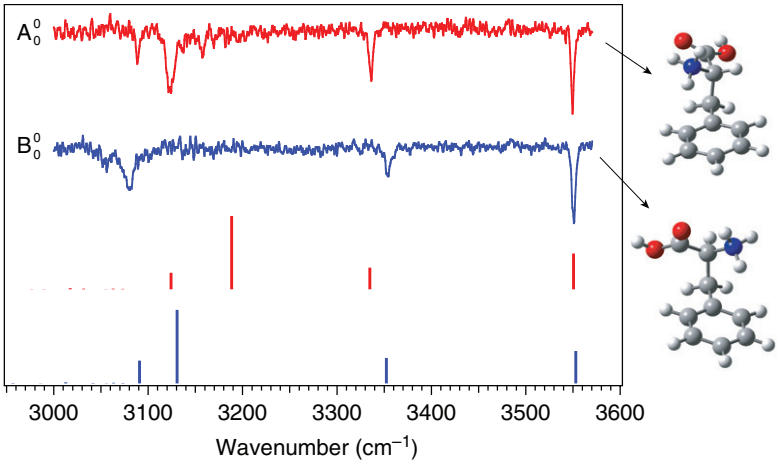

Figure 6. [Colour online] Infrared spectra of two conformers of cold of $PheH^+$ obtained with the UV laser set on the band origins A_0^0 and B_0^0 in the electronic spectrum of Figure 5. Calculated spectra (B3LYP/6-31++G**) are shown below the experimental spectra. The structures shown are those derived from the corresponding calculation. Adapted with permission from [67]. Copyright 2006 American Chemical Society.

shown in Figure 6. While the calculations do not reproduce the IR spectra exactly, they recover the important qualitative features – two of the ammonium NH stretches are strongly shifted to the red, one by interaction with the benzene ring and the other through interaction with the backbone carbonyl, while the third NH stretch is relatively unperturbed. The calculated structures differ primarily by a rotation of the side-chain about the C_α–C_β bond.

A similar treatment of $TyrH^+$ reveals four rather than two conformers and a correspondingly more complex electronic spectrum. The doubling of the number of conformers in $TyrH^+$ comes from the two possible positions of the phenol OH, which differ in energy by about 120 cm^{-1}.

Before moving on to larger peptides containing one of these chromophores, it is worth returning to the question of protonated tryptophan. The work of Kang *et al.* [89] identified the reason for the fast decay from the excited electronic state compared to $PheH^+$ and $TyrH^+$ – it comes from a low crossing barrier from the π–π^* state to a π–σ^* state that is dissociative in the NH coordinate. The difference between $TrpH^+$ in the gas phase and tryptophan in solution is nevertheless curious, in that the latter has a significant fluorescence quantum yield, implying a substantially longer lifetime. One usually expects that excited-state lifetimes will be longer in the isolated molecule compared to solution because the possibility of quenching by the solvent is removed. We investigated this difference by producing complexes of $TrpH^+$ with water in the gas phase to observe the effect of solvent in a stepwise manner [64]. Figure 7 shows the primary band in the electronic spectrum of bare protonated tryptophan together with that of the singly- and doubly-solvated species. One can clearly see a narrowing of the main band even with the addition of a single water molecule. Upon complexation with a second water molecule, the spectral features become as narrow as those of $PheH^+$ and $TyrH^+$, implying a change in lifetime of up to two orders of magnitude. As has been described in detail, this dramatic

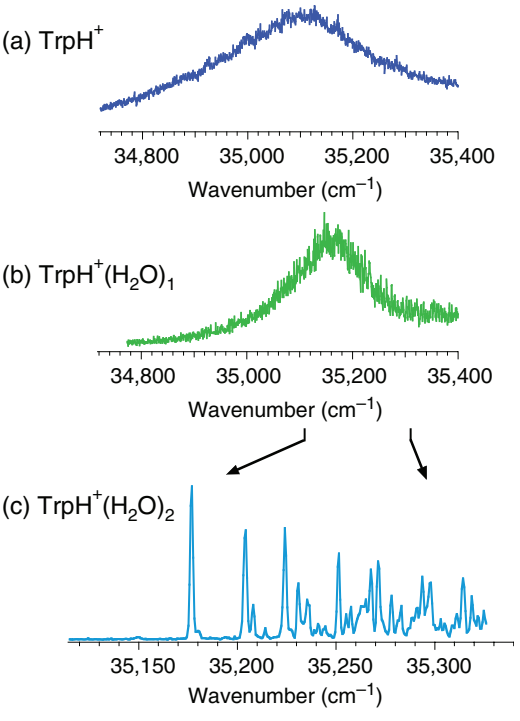

Figure 7. [Colour online] Electronic photofragment excitation spectra of $TrpH^+$ with 0, 1 and 2 attached water molecules. Reprinted with permission from [64]. Copyright 2006 American Chemical Society.

change comes from shifting the π–σ^* state relative to the π–π^* state upon solvation [64]. While the short excited state lifetime is caused by the charge on the ammonium, we have shown that it does not depend upon the charge being close to the chromophore in terms of the number of bonds, but rather by its proximity in space. This may have important implications for studies using tryptophan as a spectroscopic probe in solution when the indole ring is close to a charged group [92].

From the point of view of the development of the experimental technique, the conclusions that we can draw from these studies of protonated, aromatic amino acids are as follows:

- It is possible to cool electrosprayed ions in a 22-pole ion trap to between 11 and 16 K, which is low enough that low-frequency vibrational bands are not populated. This essentially eliminates vibrational hot-bands from the spectra.
- There is a fast decay of the indole chromophore of tryptophan in the presence of a charge. This suggests that tyrosine or phenylalanine might be better suited as spectroscopic probes of charged, gas-phase peptides.
- IR–UV double-resonance can be combined with photofragment spectroscopy to measure conformation-specific IR spectra.

We now describe the application of the same techniques to larger, more complex molecules.

4. The scaling of spectral complexity with increasing molecular size

The electronic spectra of the protonated amino acids $TyrH^+$ and $PheH^+$, while complex compared to those of small molecules typically studied by gas-phase spectroscopy, are still rather simple in that the region near the vibronic band origin is well-resolved, allowing the selection of individual conformers for measuring conformer-specific IR spectra. If one applies these techniques to molecules of increasing size, the question arises as to whether the electronic spectra will be too complex to resolve individual features.

Consider the factors that could potentially contribute to the complexity of the electronic spectrum of a large molecule:

(1) thermal inhomogeneous broadening;
(2) spectral broadening from short excited state lifetimes;
(3) a large number of Franck–Condon active low-frequency vibrations;
(4) conformational heterogeneity.

We have demonstrated that for protonated amino acids we can eliminate thermal inhomogeneous broadening through collisions with cold helium in an ion trap and that the cooling process is complete within the first 5–7 ms, after which the spectra no longer change [68]. Given that a significant number of cooling collisions continue to occur over the first 30–40 ms, it seems that the trap still has considerable unused cooling capacity. Moreover, while larger molecules contain more internal energy, the collision cross section (and hence the collision rate) with cold helium in the trap also increases, as does the number of low frequency modes through which it is easy to lose vibrational energy. Thus for fixed helium density the ultimate temperature achieved should only increase slowly with increasing molecular size.

The second factor is related the specific dynamics of the probe chromophore. We have shown that the indole chromophore of tryptophan exhibits fast excited-state decay and broadened spectra when in proximity to a charged group. While this will remain a problem, we can simply choose to use other chromophores, such as tyrosine or phenylalanine, when this factor becomes limiting.

The third factor may be an important one. The number of vibrational modes increases rapidly with the number of amino acid residues in a peptide. The question that we need to address is how many of these modes will have strong Franck–Condon activity, particularly those of low frequency that could give rise to vibrational progressions near the band origin that will prevent the resolution of individual conformers. There is some reason to believe that not all modes will appear in the spectrum. The vibrational modes that have strong Franck–Condon factors will be those for which the bond lengths and angles associated with the vibrational motion change in geometry upon excitation to the excited electronic state. Because we are using the aromatic side chains of amino acids as chromophores, one expects that most of the change in electron density in the excited state will be centred around these chromophores, and thus those bond lengths and angles near to or associated with the aromatic moiety are the ones most likely to change. Thus vibrational modes involving coordinates remote from the chromophore are unlikely to 'feel' the change in electronic excitation and hence may not appear as a vibrational progression in the electronic spectrum.

The last factor that one has to consider is conformational heterogeneity – that is, the fact that as molecules become larger the number of possible stable

conformations increases. As we cool molecules and freeze out different conformations in our ion trap, the electronic spectrum of the molecule may be extremely congested, since the precise frequency of the vibronic band origin depends upon the conformation. There is little we can argue on this point in terms of *a priori* expectations – we are simply left to try the experiment and observe the degree of complexity. Ultimately we can reduce the number of stable conformations in our ion trap by pre-selecting the ions according to their mobility in a helium buffer gas before we trap them. This work is currently being pursued in our laboratory.

To test the degree of spectral complexity in a series of molecules of increasing size, we chose peptides containing a single tyrosine chromophore and increasing numbers of alanine residues. The electronic spectra of this series of molecules are shown in Figure 8. As one can see from this progression, although the number of vibrational modes of the molecules increases by more than a factor of three, the electronic spectrum does not become significantly more complex, and the vibrational band origin seems to remain well resolved. We can draw several conclusions from this simple series of spectra, although one must be careful about generalising them. First, while there is increasing complexity with increasing size, it seems in this case not to be monotonic, and the number of Franck–Condon active vibrational modes does not seem to track the total number of vibrational modes directly. Second, the fact that the band origin remains well resolved seems to reflect the lack of extremely low frequency modes that couple to the electronic transition. While such modes certainly exist, they would have to involve the overall motion of the peptide backbone in such a way as to change the interaction with the chromophore upon vibration. The relative sparsity of the spectrum in the first $20\,cm^{-1}$ after the electronic band origin may simply mean that the lowest frequency modes do not couple to the chromophore.

Finally, the simplicity of the spectrum near the band origin also implies that there are not large numbers of different stable conformers present in the ion trap. While infrared spectra of $TyrH^+$ revealed that four conformers contributed to the electronic spectrum [67], the electronic spectrum of $H^+AlaTyr$ appears simpler, and we believe that this is due to a reduced number of stable conformations [66]. Because the molecule is more flexible, the protonated ammonium group can more easily be in contact with the aromatic ring of the tyrosine and maximise this stabilising interaction. A conformer-selected infrared spectrum of this dipeptide is shown in Figure 9, together with a calculated spectrum and the conformation giving rise to it. The close proximity of the ammonium group to the aromatic ring, which is not possible in the bare amino acid, verifies the importance of the cation–π interaction in stabilising certain conformations.

Even for the larger members of this series, the band origin does not seem to be overly congested by the presence of a large number of conformers. Whether this behaviour can be generalised to molecules of even larger size remains to be seen, but the results presented above suggests that our spectroscopic techniques can be applied to molecules at least the size of pentapeptides.

5. Spectroscopy of helical peptides

Having demonstrated that our experimental approach can generate well-resolved electronic and vibrational spectra of small peptides, we now show the results of

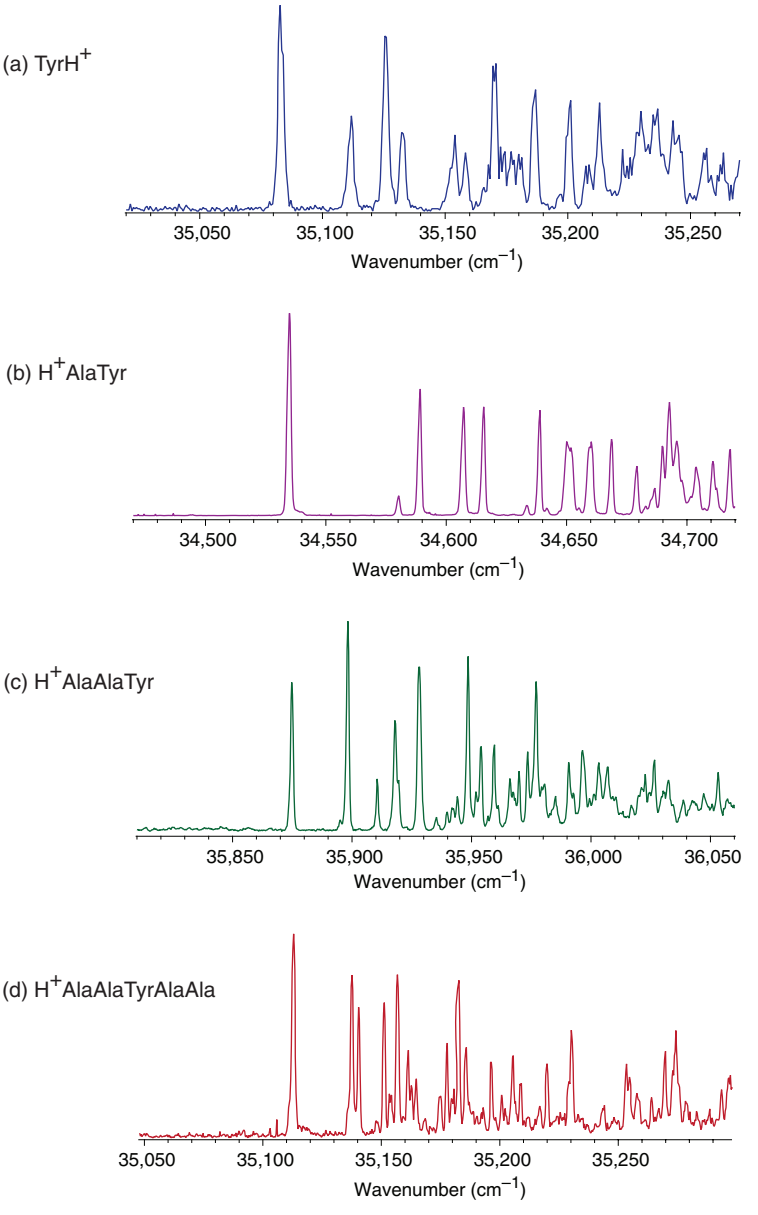

Figure 8. [Colour online] Electronic photofragment excitation spectra of a series of tyrosine-containing peptides; (a) $TyrH^+$; (b) $H^+AlaTyr$; (c) $H^+AlaAlaTyr$; (d) $H^+AlaAlaTyrAlaAla$.

applying the same techniques to a series of molecules that we expect to be helical in the gas phase [65,69,93]. The goal of this study was to identify spectroscopic signatures of helices and to test the ability of theory to predict them.

The basis of this work comes from the ion mobility studies of Jarrold *et al.* [94,95], who examined a series of alanine-containing peptides, Ac-$(Ala)_n$-$LysH^+$, Ac-$LysH^+$-$(Ala)_n$,

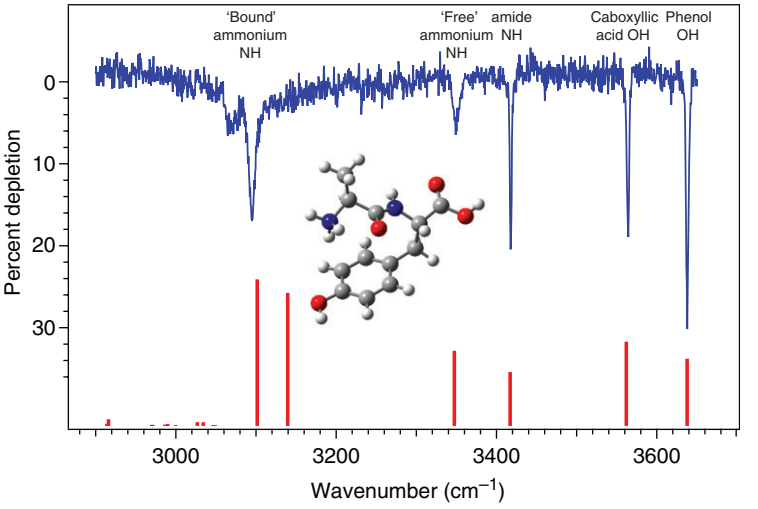

Figure 9. [Colour online] Conformer-specific IR spectrum of H^+AlaTyr recorded with the UV laser set to the electronic band origin at 34525.2 cm^{-1} together with the calculated spectrum (B3LYP/6-31++G**) and corresponding molecular structure for the lowest energy conformer.

and $(Ala)_nH^+$, as a function of the number of alanine residues, n. By measuring the relative drift times through helium, they determine the average cross section of each of these species, and in comparison with molecular dynamics calculations they can detect the difference between helical and non-helical structures. With the N-terminus protected they find that helix formation occurs only when the lysine is at the C-terminus. Putting it at the N-terminus or eliminating it altogether gives rise to non-helical structures. The protonated side-chain of the lysine plays two roles: it is involved in hydrogen bonding with three carbonyl groups on the backbone in such a way as to induce helix formation, and it stabilises the helical structure through a favourable electrostatic interaction with the helix macro-dipole.

For us to measure conformer-specific IR spectra of these alanine-based peptides we need to introduce a UV chromophore in a way that does not interfere with the formation of secondary structure, and we do this by substituting a phenylalanine for the N-terminal alanine reside. Figure 10 shows the electronic spectrum of two such peptides with lysine at the C-terminus: Ac-Phe-$(Ala)_5$-LysH^+ and Ac-Phe-$(Ala)_{10}$-LysH^+, which according to the ion mobility studies should form a helix [95], and one with lysine at the N-terminus, Ac-LysH^+-Phe-$(Ala)_{10}$, which should not form a helix.

The first thing to notice is the relative simplicity of the UV spectra in all cases. Despite the fact that these are larger than the tyrosine-containing peptides shown in Figure 8, the electronic spectra seem, if anything, even simpler. It is clear that at most a small fraction of the low-frequency vibrational modes carry strong Franck–Condon activity.

Figure 11 shows conformer-specific infrared spectra obtained by setting the UV laser at a particular band in the electronic spectrum and detecting the dips while scanning the IR OPO. The spectra of Figure 11a and b result from monitoring the two major features,

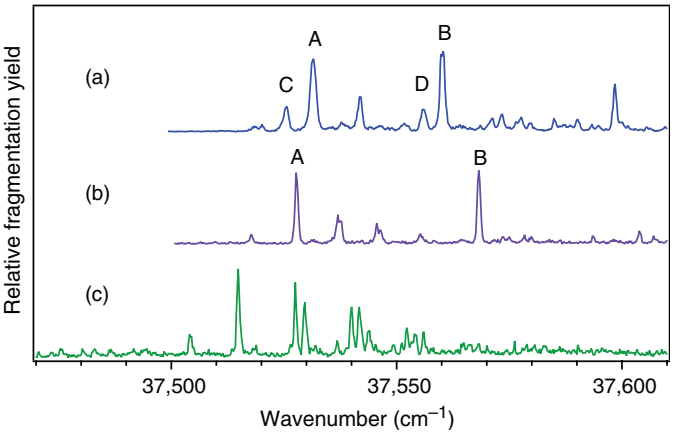

Figure 10. [Colour online] Electronic photofragment excitation spectra of (a) Ac-Phe-$(Ala)_5$-Lys-H^+, (b) Ac-Phe-$(Ala)_{10}$-Lys-H^+, and (c) Ac-LysH^+-Phe-$(Ala)_{10}$. The labels in (a) and (b) denote band origins of different conformers.

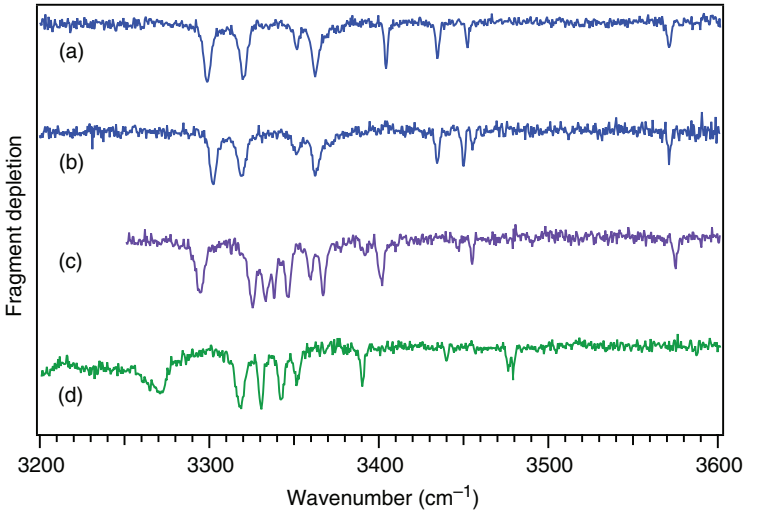

Figure 11. [Colour online] Infrared spectra of (a) conformer A of Ac-Phe-$(Ala)_5$-Lys-H^+, (b) conformer B of Ac-Phe-$(Ala)_5$-Lys-H^+, (c) conformer A of Ac-Phe-$(Ala)_{10}$-Lys-H^+ and (d) Ac-LysH^+-Phe-$(Ala)_{10}$.

marked A and B in Figure 10a, for Ac-Phe-$(Ala)_5$-LysH^+; Figure 11c is recorded with the UV laser frequency fixed on peak A in Figure 10b for Ac-Phe-$(Ala)_{10}$-LysH^+, and Figure 11d is obtained with the UV frequency set on the major peak in the spectrum of Ac-LysH^+-Phe-$(Ala)_{10}$ shown in Figure 10c. There are several important features to notice in the infrared spectra of Figure 11a and b. First, the simple fact that these spectra are different indicates that the features in the electronic spectra used to obtain them correspond to different stable conformers. One can thus distinguish conformers relatively easily using such IR spectra, even in molecules of this size.

The peak near 3575 cm^{-1} can be assigned to the free carboxylic OH stretch of the lysine at the C-terminus. The presence of a free OH stretch band is already evidence that the molecule may be helical, since if it were to adopt a globular structure, it is likely that the carboxylic OH would find itself in a hydrogen-bonding interaction that would shift the corresponding band to lower wavenumber by an amount depending upon the strength of the interaction.

The bands in the region 3300–3500 cm^{-1} arise from amide NH stretch vibrations. The appearance of seven bands in this region is consistent with fact that there are seven amide stretches and indicates that we are able to see all of them. These bands vary in both their position and their width – those shifted further to the red seem to be broader. The narrowest bands are only 2 cm^{-1} in width (before deconvolution of the OPO linewidth, which is $\sim$1cm^{-1}), while the wider amide bands approach 6 cm^{-1}. If the molecule is indeed helical, the narrow, higher frequency amide NH stretch bands are likely to be those that reside at the ends of the molecule and which do not participate in hydrogen bonding along the helix axis, whereas the red-shifted bands should come from the NH residues in the middle of the helix. This is confirmed by the observation that adding five additional alanines results in additional features in this red-shifted region, as shown in the IR spectrum of Ac-Phe-$(Ala)_{10}$-$LysH^+$ (Figure 11c). Notice also that this larger molecule still exhibits a free carboxylic acid OH stretch band, consistent with a helical structure. The three ammonium NH bands are shifted much further to the red of the spectrum shown here and are broadened by their strong interaction with the carbonyls; we typically observe them in the region of 3000–3200 cm^{-1}.

The infrared spectrum of Ac-$LysH^+$-Phe-$(Ala)_{10}$ shown in Figure 11d, while not entirely different from that of the molecules that we expect to be helical, exhibits some important differences. The free carboxylic OH stretch band is missing, and a new broad band appears near 3270 cm^{-1}, which we interpret to be a strongly hydrogen-bonded carboxylic acid OH stretch. The amide NH stretch bands in this molecule appear in the same general region of those for the previous molecules and in themselves do not allow us to distinguish between a helical and non-helical structure. However, the strong shift of the OH stretch suggests a completely different structure, since it would be difficult to construct a helix with the carboxylic OH involved in a strong hydrogen bonding interaction.

Up to this point, our interpretation of the infrared spectra of these alanine-containing peptides has been based largely on spectroscopic intuition. To be able to connect the spectra we observe to the structure of the molecule, we need to compare the positions of the spectral bands with the results of calculations. We concentrate here on the smaller of the two helical peptides, Ac-Phe-$(Ala)_5$-$LysH^+$, since it is more tractable theoretically.

Figure 12 shows measured spectra of four different conformers of Ac-Phe-$(Ala)_5$-$LysH^+$ together with calculated spectra for four of the lowest energy conformers of this molecule at the B3LYP/6-31++G** level. The vibrational bands in the calculated spectra are labelled to indicate which amino acid residue they are associated with. While an attempt has been made to compare the spectrum of each conformer with the correct calculation, this can be somewhat arbitrary, since the measured spectra do not automatically come with assignments as do the calculated spectra. When there are peaks spaced on the order of the expected accuracy of the calculations, which is the case

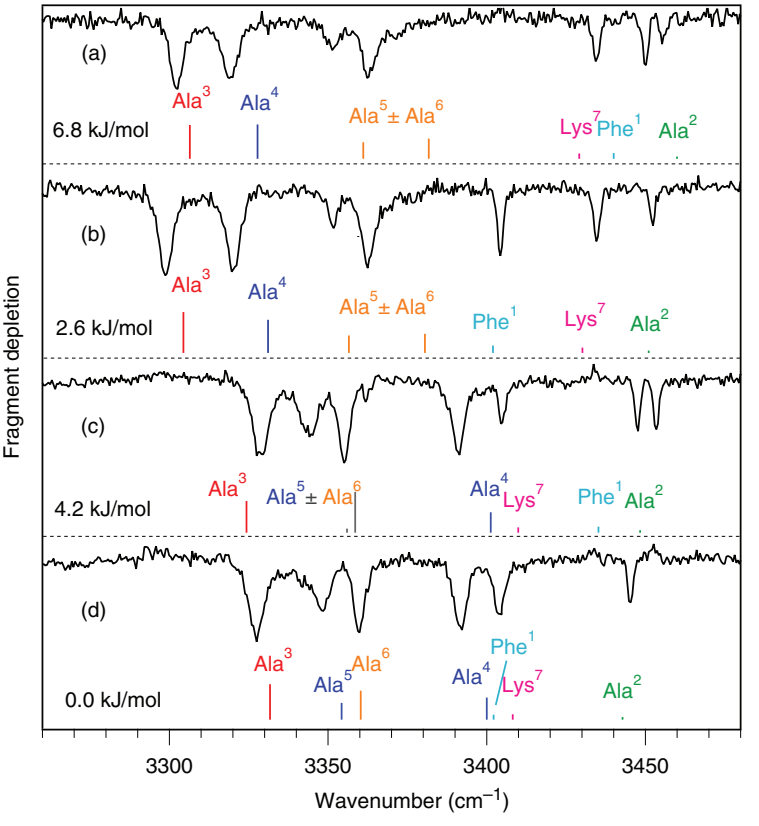

Figure 12. [Colour online] Comparison between experimental and calculated infrared spectra for conformers A-D of Ac-Phe-$(Ala)_5$-Lys-H^+ respectively in the amide NH stretch region. The best-matching calculated spectra are presented directly under each experimental spectrum together with the assignments of each peak to a specific amino acid residue.

here, there is no guarantee that the peaks we measure are ordered in the same way as the calculations. In this case a simple 'resemblance' between the measured and calculated spectra is not sufficient to associate the calculations with the measurement and assign a structure to the conformer.

The problem of assigning the measured vibrational bands to the correct amide stretches can be resolved by systematic isotopic substitution of the amide nitrogen on the different residues of the peptide. In a simple diatomic description of an amide NH stretch, substituting nitrogen-15 for nitrogen-14 would lower the NH stretch frequency by approximately 8 cm^{-1}. Figure 13 shows the spectrum of conformer B of Ac-Phe-$(Ala)_5$-LysH^+ without isotopic substitution together with the spectra with substitutions at the 2, 4 and 6 positions, counting from the N-terminus. Although we substituted only three of the seven amide nitrogens, we have measured the shifts in the spectrum of each of the four conformers, and we find that the calculated spectra do remarkably well in assigning the various vibrational bands. Of the twelve shifted bands (i.e., three in each of the four conformers), in only one case did the calculated spectrum lead to a wrong assignment, and

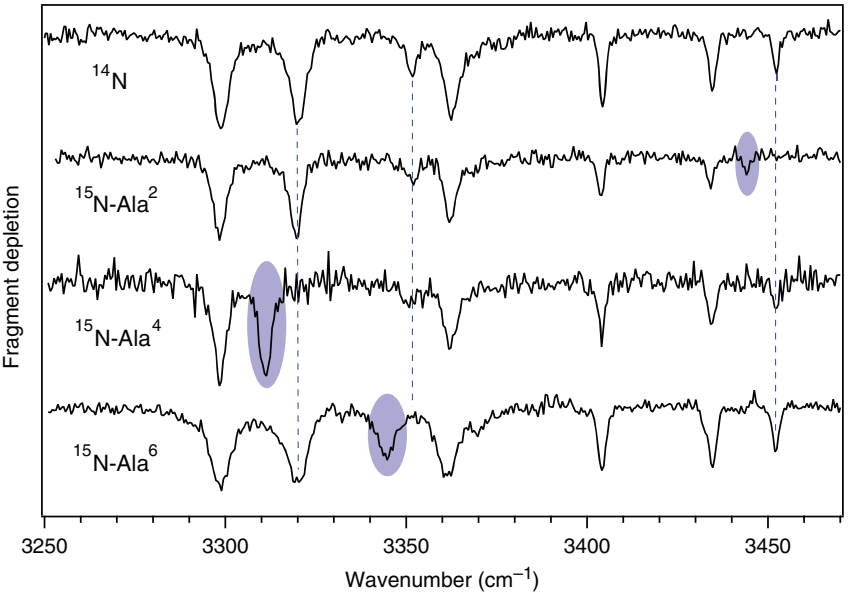

Figure 13. [Colour online] Conformer-specific IR spectra of Ac-Phe-$(Ala)_5$-Lys-H^+ with nitrogen-15 substitution at specific amino acid residues, numbered from the N-terminus. The unsubstituted peptide spectrum is shown at the top, with the singly substituted peptides shown underneath. The shifted peaks are circled, while a dashed line shows the position of those transitions in the unsubstituted peptide.

this was the reversal of Phe^1 and Ala^2 in conformer C (Figure 12c), which are less than 6 cm^{-1} apart. Overall, the verification of the calculated spectral assignments by isotopic substitution gives us confidence in attributing a particular spectrum to a specific, calculated conformer, as we have done in Figure 12.

Assuming that the comparison between the observed and calculated spectra is sufficient to allow us to assign the geometry of the conformer, we can gain insight into the interactions giving rise to a particular spectral signature. We have identified four conformers in total from the electronic spectra of Figure 10a, which we label A–D, all of which are helical, as shown in Figure 14. These conformers fall into two groups – A and B have a very similar conformation (and IR spectrum) and differ mostly by the orientation of the phenylalanine side chain, and C and D, which differ from each other in the same way. The two groups differ from each other by the hydrogen-bonding pattern of the backbone.

Beside each pair of conformers in Figure 14, we show schematically the connectivity of the hydrogen bonds implied by each structure. As one can see, the difference between the two groups of structures is the tightness of the coil – in A and B there is a series of interactions of the type C_{10}–C_{10}–C_{10}–C_{13} while in C and D it appears to be C_{10}–C_{10}–C_{13}–C_{13}. The difference between the two is simply the placement of one of the hydrogen bonds, which in the case of C and D raps the helix a bit tighter.

These hydrogen-bonding patterns allow us to rationalise some of the overall features of the infrared spectra. Indeed as we speculated earlier, the calculated geometries seem to confirm that the highest frequency NH stretch bands belong to terminal amino acid

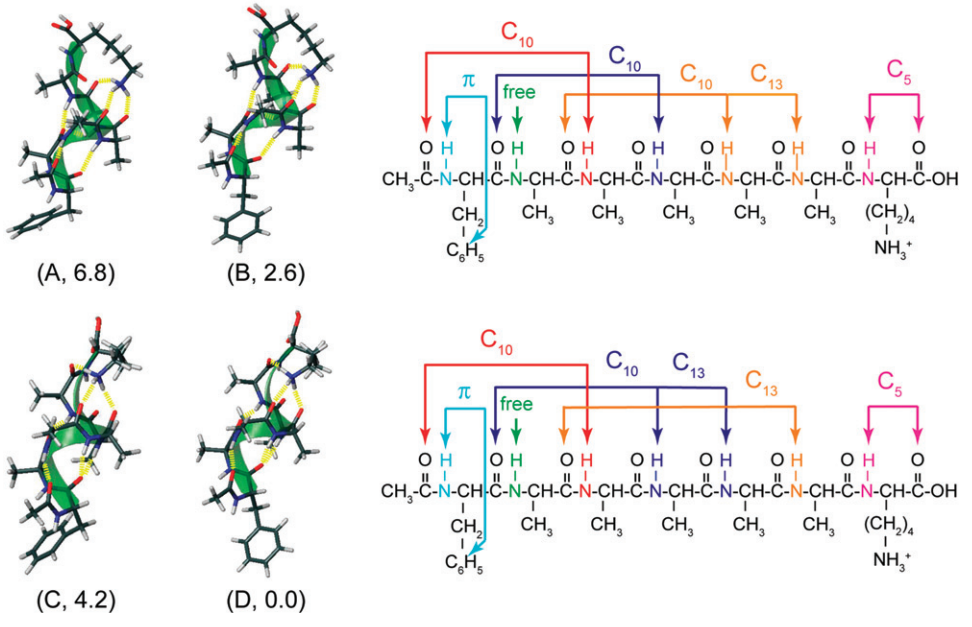

Figure 14. Calculated structures for conformers A–D of Ac-Phe-$(Ala)_5$-Lys-H^+ with the relative zero-point-corrected energies in kilojoules per mole indicated. The hydrogen bonding schemes for each pair of conformers is shown to the right.

residues that are not directly involved in the hydrogen bonding network associated with the helical backbone; namely the lysine, the phenylalanine and the first alanine from the N-terminus. The remaining amide NH bands are significantly red-shifted, although not all to the same degree. The difference between them is likely to reflect details in the CO–NH distance, the alignment of the CO and NH within the hydrogen bond and perhaps effects of cooperativity among hydrogen bonds along the helical axis. We can also see that in a helical configuration the C-terminal OH seems not to be involved in any strong hydrogen bonding interactions and should produce a free OH stretch band, which is consistent with the measured spectra.

We can also get some qualitative information about the relative energies of the different conformers. The relative intensities of the different conformer band origins in the electronic spectrum of Figure 10a carry some information on the relative energies of the conformers, but one must be careful in making a direct correlation. The intensities depend both on the conformer population and the oscillator strength for the UV transitions, and the latter can differ from one conformer to the next. Even if the band origins of different conformers were to have the same oscillator strengths, it is unlikely that the relative conformer populations (as determined by the intensities) would be related to the relative energies of the conformers in a simple way. As the molecules cool by collisions with cold helium, some will get trapped in local potential wells with barriers that divide one conformer well from another. The relative conformer populations will thus depend more on the height of the barriers to interconversion and the collisional cooling rate than on their relative energies. If this were not the case, all four conformers

would have to be extremely close in energy to have appreciable populations at a temperature of 15 K.

Despite the lack of quantitative connection between the spectral intensities for the different conformers (and hence their populations) and the conformer energy, we can deduce the relative energy ordering, since the lower energy conformers should be more highly populated. Barring any dramatic difference in oscillator strength for the relative band origins, the electronic spectrum of Figure 10a would predict that conformers A and B are the lowest in energy followed by C and D. This is different than our calculations, which predicts energies of 6.8, 2.6, 4.2, and 0 kJ/mol for conformers A–D, respectively (Figure 12). A detailed systematic study of computational methods is needed to resolve this discrepancy between theory and experiment.

It seems clear that conformer-specific infrared spectra are able to distinguish the two classes of conformers – A and B compared to C and D. This is enabled largely by the high resolution afforded by the cooling in our ion trap since much of this structure would be hidden in room temperature spectra. While the comparison here between experiment and theory is far from perfect, the high-resolution spectra that can be obtained using this approach provide an important benchmark for theory, particularly since the complicating effects of solvent are eliminated.

6. Toward still larger molecules

We have demonstrated the ability to measure highly resolved infrared spectra of small gas-phase peptides, which provide a benchmark for theoretical calculations. Even though high-resolution spectra of molecules of this size may push the limits of theory, there are reasons for us to want to apply these techniques to still larger molecules. Peptides of up to 10–12 amino-acids described above are at the lower limit of what is required to fully develop secondary structure – moving to still larger molecules would perhaps further stabilise such structural features and allow us to observe elements of tertiary structure such as interacting helices. Moreover, it is more likely that larger molecules will retain something that resembles their condensed-phase structure in the gas phase since the accumulation of many non-covalent interactions will make a considerable contribution to the overall stabilisation energy. Our ultimate goal is to be able to extract useful structural information, even if it is only qualitative, on naturally occurring peptides and proteins.

The first question that arises is whether the spectra of still larger molecules will be simple enough to extract any information. The UV spectrum of Ac-Phe-$(Ala)_{10}$-$LysH^+$, the largest of the molecules discussed above, is uncongested and allows us to measure conformer-specific IR spectra without difficulty. While not fully resolved under the conditions that we employ, these IR spectra could be further resolved with improvements in our IR laser resolution. As we move to larger molecules, at some point a large distribution of stable conformers, which we have not observed until now, might become the major source of spectral congestion. Once conformational heterogeneity becomes the limiting factor, combining our techniques with other experimental methods, such as ion mobility, might help reduce the problem. For the moment, our goal is to explore the limits of our current techniques.

Putting aside for the moment questions of spectral complexity, if we wish to push these techniques to still larger molecules, there are two questions that must be addressed from an experimental point of view:

- Will we be able to dissociate larger molecules with a single UV photon for photofragment-based detection?
- Will infrared depletion spectroscopy work on larger molecules?

We present here some of our most recent experimental developments that allow us to address these questions [70].

The use of spectroscopic techniques based on UV photofragmentation requires that the molecules initially promoted to an excited electronic state will dissociate on a short enough timescale compared to competing processes. If the molecules dissociate directly from an excited electronic state, the process is typically fast, and the lifetime should not scale with molecular size. In this case, the techniques described above might work perfectly well on larger molecules. However, if the dissociation occurs first by internal conversion to the ground electronic state followed by statistical vibrational energy redistribution and unimolecular dissociation, the lifetime of the molecule could scale strongly with the number of vibrational modes. If this were the case, processes that compete with unimolecular dissociation, such as collisional relaxation by residual helium in the ion trap or infrared fluorescence, might reduce the fraction of molecules that dissociate, rendering photofragment spectroscopy of large species difficult if not impossible.

In the experiments described thus far, the cadence of the experiment was determined by the laser repetition rate. The trapping cycle is repeated every 50 ms, and depending upon the specific experiment, the lasers operate at either 10 or 20 Hz. During a typical trapping cycle, the molecules cool in collisions with helium during the first 10 ms, and then we leave up to 30 ms for the helium to be pumped away. Since we excite the molecules with a UV laser pulse 40 ms into the trapping cycle, this leaves at most 10 ms for them to dissociate. To extend this time, we could run the lasers and the trapping cycle at half the repetition rate or less, and this would allow up to 100 ms for the molecules to dissociate, albeit at the expense of the duty cycle of the experiment. Unfortunately, on this timescale, radiative cooling can become significant and may compete with dissociation.

To deal with this problem we apply a technique similar to one we used in the past for photofragment spectroscopy of weak vibrational overtone transitions, which we called infrared laser-assisted photofragment spectroscopy (IRLAPS) [96–98]. The basic idea as applied to the current experiments is illustrated in Figure 15 [70]. Suppose that after UV excitation of a large, gas-phase peptide, unimolecular dissociation is slow, and only a small fraction of the molecules produce fragments in the time before the trap is emptied. By introducing a CO_2 laser pulse subsequent to the UV pulse, we can induce infrared multiphoton excitation of the pre-excited peptide molecules, increasing their vibrational energy and hence their dissociation rate. This should cause a significantly larger fraction of molecules to dissociate during the fixed time before the trap is emptied.

For this approach to work, the CO_2 laser pulse must selectively excite only those molecules that are first promoted to the excited electronic state and not those that remain in the ground electronic state. If this is achieved, an electronic spectrum can be recorded in the same way as before – by observing the fragment ion signal as a function of the UV laser frequency. There are two factors that may allow us to selectively dissociate only those

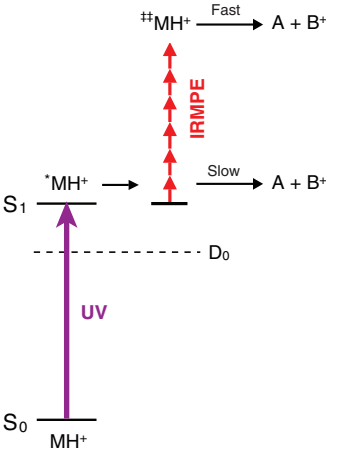

Figure 15. [Colour online] Excitation scheme for the application of IRLAPS for measuring the electronic spectrum of large, protonated biomolecular ions.

molecules that have first undergone UV pre-excitation, similar to the situation in our previous work on small, vibrationally-excited polyatomic molecules [96,97]. First, since the pre-excited molecules already have on the order of 37000 cm^{-1} of internal energy, they need to absorb fewer photons from the CO_2 laser (compared to those not receiving the UV excitation) to reach an energy at which the dissociation rate becomes sufficiently fast. We can therefore use the CO_2 laser fluence as a parameter to discriminate against dissociating unexcited molecules, since at sufficiently low fluence they will not gain enough energy. The second factor relates to the CO_2 laser frequency used. Because the ions in our trap are cold, their infrared absorption in the CO_2 laser region should be sharp, whereas those that have first been excited with the UV laser and undergone internal conversion are internally warm. If we tune the CO_2 laser away from a resonant frequency of the cold, ground state molecules, excitation of these molecules by the CO_2 laser alone should be inefficient, while the internally warm pre-excited molecules should have broad infrared absorption and be preferentially pumped by the CO_2 laser.

As a demonstration of this technique, we show in Figure 16 electronic photofragment excitation spectra of a seventeen amino acid peptide, Ac-Phe-$(Ala)_7$-$LysH^+$-$(Pro)_2$-$(Ala)_5$-Lys H^+, obtained with only the UV excitation laser and with the addition of the CO_2 laser [70]. In the former case we observe less that one fragment ion per laser pulse, even on the strongest peaks, but as shown in the figure, this increases by over two orders of magnitude when assisted by the CO_2 laser.

Having demonstrated the effectiveness of this approach for electronic spectroscopy, we now consider whether we can use it to measure conformer-selective infrared spectra. In this case, an IR spectroscopic laser would precede the UV laser in the same way as for the smaller systems described above, and the infrared absorption would be detected as a dip on the fragment ion signal. There are two questions related to the successful implementation of this approach that need to be addressed. First, can the CO_2 laser dissociate selectively only those molecules promoted to the excited electronic state and not those first excited with infrared radiation? After absorption of the IR photon for the spectroscopic

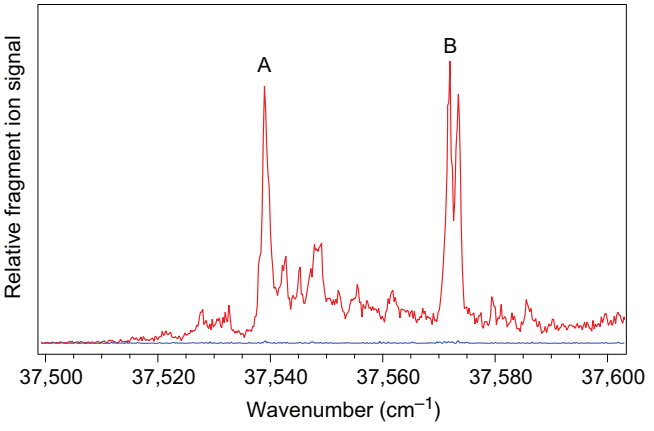

Figure 16. [Colour online] Electronic spectrum of Ac-Phe-$(Ala)_7$-$LysH^+$-$(Pro)_2$-$(Ala)_5$-$LysH^+$ obtained (a) by UV photofragment spectroscopy (blue line), and (b) by IRLAPS in which the UV excitation is assisted by infrared multiphoton excitation by a CO_2 laser (red line). In both cases the fragment with m/z of 710 is monitored. The CO_2 laser was tuned to the 9P(16) line at 1050.1 cm^{-1}.

excitation, the molecule becomes internally warm, and the absorption spectrum in the region of the CO_2 laser will no longer be sharp. This simply leaves the possibility to discriminate only on the basis of the CO_2 laser fluence and not its frequency. The second question is whether in such a large molecule the infrared absorption will cause a dip in the UV-induced fragmentation. As the molecule becomes larger with more vibrational modes, the degree of internal warming caused by the IR excitation and the accompanying spectral broadening responsible for the dip in the UV spectrum, should decrease.

Figure 17 shows two infrared spectra of the seventeen amino acid peptide Ac-Phe-$(Ala)_7$-$LysH^+$-$(Pro)_2$-$(Ala)_5$-Lys H^+ recorded with the UV laser set on the peaks labelled A and B in the electronic spectrum of Figure 16 [70]. The degree of depletion achieved by the IR spectroscopic laser is as much as 62%, which clearly indicates that the CO_2 laser can selectively dissociate the electronically excited molecules. Moreover for a molecule this size, adding on the order of 3400 cm^{-1} of vibrational excitation is still sufficient to broaden and shift the electronic spectrum to result in a dip at the UV probe frequency, allowing us to measure an infrared spectrum. Although these spectra are not completely resolved, one can clearly see that they are distinctly different, indicating that the features in the UV spectrum arise from different stable conformers.

The application of IRLAPS to UV photofragment spectroscopy of larger biological molecules is still in its infancy and there are many questions about the mechanism that still need to be addressed. While we expected that dissociation of UV-excited ions would normally proceed on the ground electronic potential energy surface in a statistical manner, there are two observations that suggest that this may not be the case. The first is the fact that the fragmentation channel that seems always to be most enhanced by infrared multiphoton excitation in the IRLAPS scheme is the loss of the neutral aromatic side chain by cleavage of the C_α–C_β bond, despite the fact that it is not the weakest bond in the molecule. We deduce the latter from our observation that in collision-induced dissociation and in IRMPD of the parent molecules, both of which should proceed on the ground

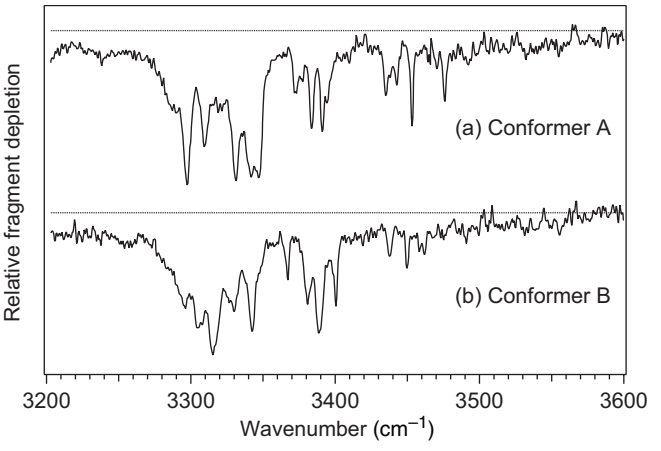

Figure 17. Conformer-specific IR spectra of Ac-Phe-$(Ala)_7$-$LysH^+$-$(Pro)_2$-$(Ala)_5$-$LysH^+$ obtained by depleting the IRLAPS signal with the UV laser set on the features marked A and B in Figure 16. Adapted with permission from [70]. Copyright 2006 American Chemical Society.

electronic surface, breakage of the $C_\alpha - C_\beta$ bond is a minor channel. Secondly, the fragmentation appears to occur promptly after CO_2 laser excitation, since the dissociation yield does not drop when we shorten the time allowed for dissociation. We would expect that if dissociation occurred in a statistical manner from highly excited levels of the ground electronic state, the rate would get progressively slower with increasing size of the molecule. Our observations suggest that the dissociation induced by the CO_2 laser may occur on an excited electronic surface or in an intermediate species that is promptly formed after UV excitation. While the dissociation mechanism in the IRLAPS scheme continues to be a subject of study in our laboratory, the open questions might be best addressed by the powerful coincidence techniques of Jouvet *et al*. [99–101].

7. Limitations and future directions

In this section we consider potential limitations to our present technique, methods that might be used to overcome such limitations as well as possible extensions to the technique that we can envisage for the future that would provide even more detailed information.

It is clear that as we push to larger molecules, both the electronic and vibrational spectra will eventually become more complex. Complexity in the electronic spectra will limit our ability to measure conformer-specific infrared spectra. If the infrared spectra themselves are too congested, they may still serve as a fingerprint of the molecule, but the comparison with theory will be difficult, and hence it will be difficult to extract detailed information about the nature of the forces that drive a molecule to adopt a particular conformation. The factors that limit these two types of spectra are slightly different.

For electronic spectra, if we assume that we can continue to cool larger molecules efficiently, which eliminates thermal inhomogeneous broadening, the remaining possible sources of spectral congestion are a larger number of Franck–Condon active low-frequency vibrations and a large number of stable conformers with slightly different electronic spectra. As discussed previously, the first of these factors is difficult to estimate *a priori*.

While one can estimate the number of low frequency vibrations, it is difficult to predict which ones will have strong Franck–Condon activity. However, there is reason to believe that this problem will remain manageable, since the vibrational modes that change geometry in the excited state should only be those near the chromophore.

The problem of conformational heterogeneity will likely become a serious problem for molecules significantly larger than those presented here. The use of 'multi-dimensional' techniques in spectroscopy has proven to be a powerful way to remove heterogeneous broadening. In the work described above, we used IR–UV double-resonance to allow conformer specific IR spectra. Using higher orders of multiple resonance such as IR–IR–UV schemes [42] should allow extensions to more complex systems. However, one could imagine other 'dimensions' in which to distinguish the spectra of different conformers. For example, the combination of ion mobility techniques, which can first select a certain family of conformations by their mobility in drifting through a finite pressure of bath gas, with the kind of ion-trap spectroscopy described here should be able to reduce the number of features in an electronic spectrum by physically separating the conformers before injection into the trap.

An additional source of spectral complexity in electronic spectra will arise as we begin to examine naturally occurring peptides and proteins, which are likely to contain multiple aromatic amino acids. The transitions centred on these distinct chromophores may overlap and interact, particularly when the chromophores are of the same type. Interactions between different chromophores do not in themselves pose a problem, as the electronic spectrum is simply used to perform conformer selection, however the overlap of spectra may inhibit conformer selection. This is clearly an inherent limitation of using naturally occurring chromophores, which is no different from problems experienced in solution, where some studies have concentrated on proteins with a single tryptophan residue. One solution would be to introduce non-natural chromophores into a peptide or protein in such a way that does not perturb the overall structure of the molecule. These could be chosen to have electronic absorptions distinct from the aromatic amino acids.

The question of complexity in the *infrared* spectra is closely tied to our ability to select single conformations *via* an electronic excitation and then use IR–UV double resonance; hence the two types of spectra are not completely independent. However, even if electronic spectra are simple enough to allow the selection of a single stable conformation, it does not guarantee that the vibrational spectrum will be simple, since large molecules, particularly those with repeating units such as peptides, will have a large number of vibrational bands in similar environments that will overlap. Exactly how many vibrational bands appear in a spectrum depends upon the mechanism of IR–UV double resonance. As described in much of the work on neutral molecules, the dip in a fluorescence or ion signal upon IR excitation comes from depopulation of the initial state that is tagged by a UV transition. The language commonly used to describe this process assumes that once vibrationally excited, the molecules no longer absorb the UV laser at the same frequency, and this causes a dip in the signal. However it is important to understand why the UV absorption frequency shifts once a molecule is vibrationally excited. If the shift comes from a coupling between the vibrational and electronic excitations, then the vibrational bands that cause a dip in the UV signal will be those that have strong Franck–Condon factors for $\Delta v \neq 0$ transitions in the electronic transition. In other words, if the molecules are excited to a particular $v = 1$ vibrational level and that mode has a strong Franck–Condon factor for a $\Delta v = 0$

transition, the electronic absorption will not be very different from the ground state molecules, and the IR absorption will not result in a depletion of the photofragmentation signal. If, on the other hand, the molecules are excited to the $v = 1$ level of a vibrational mode with a weak $\Delta v = 0$ Franck–Condon factor, the electronic absorption will be weaker than that for unexcited molecules, and the photofragment signal will dip. If this is the correct interpretation, then one might expect that only a small subset of vibrational modes will contribute to the infrared spectrum – that is, modes in the vicinity of the UV probe chromophore for which one might expect a geometry change upon electronic excitation. However, this interpretation implicitly assumes that there is no intramolecular vibrational energy redistribution on the timescale of the delay between the IR pump and UV probe lasers. Since the delay is typically 200 ns, this prospect seems unlikely. A more likely scenario is that after IR excitation, the vibrational energy redistributes among the vibrational modes of the molecule, putting it in states of mixed vibrational character. Such states will have components of their wave functions that represent population in many low frequency vibrational modes since the density of states of this type is the highest. The UV spectrum of a molecule in such states will be broadened by what is sometimes referred to as 'statistical inhomogeneous broadening' [102,103], which comes about because the different components of the mixed wave function will give rise to slightly different UV absorption frequencies. Because the UV spectrum is broadened compared to the cold, unexcited molecule, the intensity of UV absorption will be lower at the resonant frequency of the cold molecule, and thus one observes a dip. While the result may appear the same as if we simply removed population from the ground state and assumed no intramolecular vibrational energy redistribution, the scaling of the complexity of the infrared spectrum with molecular size will depend on the mechanism responsible for the IR-induced dip. If the vibrational energy is statistically distributed after IR excitation, then all vibrational modes of the molecule will appear in the IR dip spectrum. This means that the complexity of the vibrational spectrum will continue to increase with the size of the molecule and that the IR spectrum will not be a local probe of the chromophore region. Moreover, as the molecule gets larger, the excited vibrational state will consist of a wider mixture of states involving modes further from the chromophore. Because these modes will tend to have strong Franck–Condon factors for $\Delta v=0$ transitions, the degree of broadening will decrease roughly in proportion to $1/(\mathrm{SQRT}(S))$, where S is the number of mixed states. This implies that with increasing molecular size the degree of dip in the spectrum will decrease, making it increasingly difficult to measure IR spectra. Exactly what size molecule is required to put us in that regime is not completely clear. At least for peptides of seventeen amino acids, the amide NH stretch bands appear with significant intensity.

While one of the primary goals of these experiments is to test theory, the need for theory to provide the connection between the measured vibrational spectrum and molecular structure is perhaps one of our ultimate limitations to using the data. The connection between theory and experiment is discussed in more detail below.

8. State of comparison with theory

We have presented the results of reasonably complete DFT calculations at the B3LYP/6-31++G** level for the protonated amino acids and B3LYP/6-31G** for Ac-Phe-$(Ala)_5$-$LysH^+$. Although these calculations, with assistance from isotopic labelling, allowed us to

assign individual transitions to particular oscillators and to connect the spectra to specific conformations, we still found disagreements between theory and experiment. Moreover, we were unable to apply these same methods to the larger molecules discussed in this review. This section outlines the strengths and weaknesses of our chosen procedures, suggests methods that might improve on the current results, and discusses the difficulties encountered as we move to larger molecules.

The first step in obtaining a set of calculated geometries and frequencies is to use a low level of theory to identify candidate structures for further analysis. We employ a random search method for conformational searching using the AMBER force field. In the case of Ac-Phe-$(Ala)_5$-$LysH^+$ we generated 50,000 structures, of which just over 1000 were unique and within 50 kJ/mol of the most stable structure. When we calculated the energies of these conformations using B3LYP/6-31G**, the energy ordering changed considerably. For example, the global minimum conformation of Ac-Phe-$(Ala)_5$-$LysH^+$, according to DFT (assigned as conformer D) was the 35th lowest energy conformation according to AMBER. However, when the conformations were fully optimised with DFT, further reordering was minimal. Thus, while the AMBER force field calculates geometries that do not change much at higher levels of theory, the energy ordering is not as reliable. The problem of correctly selecting low-energy conformations with force field methods likely becomes more difficult in systems other than these helices, which seem to be particularly stable [94]. Because the random search procedure uses low-energy structures to generate new structures during the search, and because the helices are so much lower in energy than other types of structures, the search procedure will stay mostly within the helical regime, allowing it to fully explore that small region of conformation-space that accounts for all of the low-energy conformations. By contrast, a potential energy surface with a wider variety of structures within a smaller energy window may not be as thoroughly explored within the same number of iterations.

Once a set of candidate structures have been identified by force field searches, we then employ higher-level calculations to find the very lowest minima, and to calculate harmonic vibrational frequencies. We employ the B3LYP functional with a 6-31++G** basis for smaller systems and 6-31G** for larger ones. In previous sections, we have identified two weaknesses with our DFT calculations: the energy ordering for Ac-Phe-$(Ala)_5$-$LysH^+$ does not match the apparent conformational populations seen in the spectra; and there is still substantial error in the calculated frequencies compared to the experiment. We look at these factors in turn.

As discussed above, one should use caution when assuming conformer populations based on UV spectra because of possible differences in transition strengths for the different conformers. If we assume that the UV spectrum reflects the actual populations, the precise ordering of the lowest energy conformations in Ac-Phe-$(Ala)_5$-$LysH^+$ does not appear correct. We should emphasise, however, that the four observed conformations are among the five lowest calculated, implying that DFT *does* recover the overall energetics reasonably well. The detailed differences may be due to the well-known lack of dispersion in DFT. In smaller molecules containing aromatic rings and amide groups, the interaction between the two can be an important stabilising factor that determines the lowest energy conformations [24]. In helices, this type of interaction is much less important than hydrogen bonding, but the complete omission of dispersion interactions may account for differences of several kilojoules per mole.

On the whole, the scaled DFT harmonic frequency calculations are good enough to allow us to relate a structure to the measured spectra for the protonated aromatic amino acids and for Ac-Phe-$(Ala)_5$-$LysH^+$, and to identify particular weaknesses in the theory. The IR spectra of $PheH^+$ (Figure 6) point out a recurring weakness – the poor calculation of hydrogen-bonded ammonium NH stretches. Calculations using MP2 provided no improvement to these frequencies, ruling out dispersion as the source of the problem. Anharmonic frequencies, on the other hand, improved the agreement substantially with the added advantage of requiring no scale factor. We thus concluded that anharmonicity in hydrogen-bonded ammonium NH stretches is so large that normal harmonic methods, even when scaled, were insufficient to determine accurate frequencies. The calculation of conformations A and B of Ac-Phe-$(Ala)_5$-$LysH^+$ point to a second flaw in this level of theory – the coupling between the NH stretches of Ala^5 and Ala^6 [65,69]. The calculations suggest vibrations that are the symmetric and antisymmetric combinations of the two local oscillators, with nearly equal intensity and a substantial spacing between them, while the experiment shows two vibrations with markedly unequal intensity and only a slight splitting. Larger molecules are likely to have many coupled oscillators, and thus correct prediction of this interaction is crucial. In general, the mismatch between the calculated and experimental frequencies will become problematic for larger molecules with congested spectra and smaller differences between conformations.

There are several options for improvements to the calculations we have discussed here. The shape of the potential energy surface is, of course, the primary factor in the accuracy of the energies and the frequencies, so improvements in DFT and inclusion of dispersion in future calculations will ameliorate this to some degree [104–109]. Moving to higher levels of theory than DFT may also be a necessary step. The computational expense of MP2 has precluded its general use in the size of molecules we study, but the development of the resolution-of-the-identity (RI) approximation offers a less expensive route to MP2 energies [110]. Finally, it is clearly necessary to include anharmonicity in the frequency calculations, but this remains quite expensive.

The methods outlined here that worked well for Ac-Phe-$(Ala)_5$-$LysH^+$ were too computationally expensive for application to Ac-Phe-$(Ala)_{10}$-$LysH^+$. The use of the RI approximation with DFT offers an order-of-magnitude reduction in computation time for optimisations and frequency calculations of molecules the size of Ac-Phe-$(Ala)_{10}$-$LysH^+$. For example, we have found that frequencies can be calculated for Ac-Phe-$(Ala)_{10}$-$LysH^+$ at the RI-BP86/SVP level of theory in approximately the same time as a frequency calculation of Ac-Phe-$(Ala)_5$-$LysH^+$ at the B3LYP/6-31G** level. However, we used Ac-Phe-$(Ala)_5$-$LysH^+$ to test the accuracy of RI-BP86/SVP frequencies, and found a worse match to our experimental frequencies than with B3LYP/6-31G**. Employing a larger basis set gave better frequencies, but even RI-BP86/TZVP was prohibitively expensive for Ac-Phe-$(Ala)_{10}$-$LysH^+$. Continued refinement of basis sets, functionals, and time-saving approximations will aid the field of large-molecule high-resolution spectroscopy immensely.

9. Conclusions

In this review we have tried to demonstrate the potential of the techniques that we have developed for obtaining conformation-specific IR spectra of cold biomolecular ions. The combination of electrospray ionisation for producing gas-phase peptides, ion-trapping

techniques to cool and confine them and multiple-laser spectroscopic schemes enable the measurement of highly resolved electronic spectra of these species. Using such spectra to identify electronic transitions from different conformers permits the measurement of conformer-specific IR spectra, which, in comparison with calculations, allows us to identify the geometry of the molecules. The particular class of molecules discussed here was chosen because of their propensity to form gas-phase helices, allowing us to investigate the spectral signatures of this secondary structural element. The highly resolved spectra for such species provide stringent benchmarks for theory. If one is to have confidence in theoretical calculations on molecules even larger than these in more complex environments, such calculations must be able to reproduce the spectra obtained here in the well-defined and controlled environment of a cold ion trap. It is our hope that such benchmark experiments can help provide the means to improve theoretical approaches.

The continued development of these techniques requires a detailed understanding of the sources of complexity in the electronic spectra of large molecules, the photophysics of biological chromophores in their excited electronic states and the dynamics of intramolecular vibrational energy distribution in the ground electronic state, and these are subjects that are currently under investigation in our laboratory.

Acknowledgements

We gratefully acknowledge and thank the École Polytechnique Fédérale de Lausanne and the Fond National Suisse (grant no. 200020-112071) for their generous support of this work. The studies discussed in this article are the result of the work of many talented group members: Sebastien Mercier, Monia Guidi, Caroline Seaiby, Ulrich Lorenz and Georgios Papadopoulos.

References

[1] T. R. Rizzo, Y. D. Park, and D. H. Levy, J. Am. Chem. Soc. **107**, 277 (1985).
[2] T. R. Rizzo, Y. D. Park, and D. H. Levy, J. Chem. Phys. **85**, 6945 (1986).
[3] T. R. Rizzo, Y. D. Park, L. Peteanu, and D. H. Levy, J. Chem. Phys. **83**, 4819 (1985).
[4] T. R. Rizzo, Y. D. Park, L. A. Peteanu, and D. H. Levy, J. Chem. Phys. **84**, 2534 (1986).
[5] J. R. Cable, M. J. Tubergen, and D. H. Levy, J. Am. Chem. Soc. **109**, 6198 (1987).
[6] J. R. Cable, M. J. Tubergen, and D. H. Levy, Faraday Discuss. **86**, 143 (1988).
[7] J. R. Cable, M. J. Tubergen, and D. H. Levy, J. Am. Chem. Soc. **110**, 7349 (1988).
[8] L. A. Philips and D. H. Levy, J. Chem. Phys. **89**, 85 (1988).
[9] J. R. Cable, M. J. Tubergen, and D. H. Levy, J. Am. Chem. Soc. **111**, 9032 (1989).
[10] A. G. Szabo and D. M. Rayner, J. Am. Chem. Soc. **102**, 554 (1980).
[11] M. C. Chang, J. W. Petrich, D. B. McDonald, and G. R. Fleming, J. Am. Chem. Soc. **105**, 3819 (1983).
[12] J. W. Petrich, M. C. Chang, D. B. McDonald, and G. R. Fleming, J. Am. Chem. Soc. **105**, 3824 (1983).
[13] Y. D. Park, T. R. Rizzo, L. A. Peteanu, and D. H. Levy, J. Chem. Phys. **84**, 6539 (1986).
[14] L. A. Peteanu and D. H. Levy, J. Phys. Chem. **92**, 6554 (1988).
[15] E. Nir, H. E. Hunziker, and M. S. de Vries, Anal. Chem. **71**, 1674 (1999).
[16] R. Cohen, B. Brauer, E. Nir, L. Grace, and M. S. de Vries, J. Phys. Chem. A **104**, 6351 (2000).
[17] C. Unterberg, A. Gerlach, T. Schrader, and M. Gerhards, J. Chem. Phys. **118**, 8296 (2003).
[18] W. Chin, M. Mons, J. P. Dognon, F. Piuzzi, B. Tardivel, and I. Dimicoli, Phys. Chem. Chem. Phys. **6**, 2700 (2004).

[19] H. Fricke, A. Gerlach, C. Unterberg, P. Rzepecki, T. Schrader, and M. Gerhards, Phys. Chem. Chem. Phys. **6**, 4636 (2004).
[20] I. Hunig and K. Kleinermanns, Phys. Chem. Chem. Phys. **6**, 2650 (2004).
[21] J. M. Bakker, C. Plutzer, I. Hunig, T. Haber, I. Compagnon, G. von Helden, G. Meijer, and K. Kleinermanns, Chem. phys. chem. **6**, 120 (2005).
[22] W. Chin, I. Compagnon, J. P. Dognon, C. Canuel, F. Piuzzi, I. Dimicoli, G. von Helden, G. Meijer, and M. Mons, J. Am. Chem. Soc. **127**, 1388 (2005).
[23] W. Chin, J. P. Dognon, F. Piuzzi, B. Tardivel, I. Dimicoli, and M. Mons, J. Am. Chem. Soc. **127**, 707 (2005).
[24] D. Reha, H. Valdes, J. Vondrasek, P. Hobza, A. Abu-Riziq, B. Crews, and M. S. de Vries, Chem-Eur. J. **11**, 6803 (2005).
[25] V. Brenner, F. Piuzzi, I. Dimicoli, B. Tardivel, and M. Mons, J. Phys. Chem. A **111**, 7347 (2007).
[26] T. Haber, K. Seefeld, and K. Kleinermanns, J. Phys. Chem. A **111**, 3038 (2007).
[27] H. Fricke, G. Schafer, T. Schrader, and M. Gerhards, Phys. Chem. Chem. Phys. **9**, 4592 (2007).
[28] A. Abo-Riziq, B. O. Crews, M. P. Callahan, L. Grace, and M. S. de Vries, Angew. Chem. Int. Edit. **45**, 5166 (2006).
[29] M. S. de Vries and P. Hobza, Annu. Rev. Phys. Chem. **58**, 585 (2007).
[30] J. R. Carney and T. S. Zwier, J. Phys. Chem. A **104**, 8677 (2000).
[31] L. C. Snoek, E. G. Robertson, R. T. Kroemer, and J. P. Simons, Chem. Phys. Lett. **321**, 49 (2000).
[32] J. R. Carney and T. S. Zwier, Chem. Phys. Lett. **341**, 77 (2001).
[33] T. S. Zwier, J. Phys. Chem. A **105**, 8827 (2001).
[34] L. C. Snoek, R. T. Kroemer, M. R. Hockridge, and J. P. Simons, Phys. Chem. Chem. Phys. **3**, 1819 (2001).
[35] B. C. Dian, A. Longarte, S. Mercier, D. A. Evans, D. J. Wales, and T. S. Zwier, J. Chem. Phys. **117**, 10688 (2002).
[36] G. M. Florio and T. S. Zwier, J. Phys. Chem. A **107**, 974 (2003).
[37] P. Carcabal, R. T. Kroemer, L. C. Snoek, J. P. Simons, J. M. Bakker, I. Compagnon, G. Meijer, and G. von Helden, Phys. Chem. Chem. Phys. **6**, 4546 (2004).
[38] W. Chin, J. P. Dognon, C. Canuel, F. Piuzzi, I. Dimicoli, M. Mons, I. Compagnon, G. von Helden, and G. Meijer, J. Chem. Phys. **122**, 054317 (2005).
[39] W. Chin, F. Piuzzi, J. P. Dognon, L. Dimicoli, B. Tardivel, and M. Mons, J. Am. Chem. Soc. **127**, 11900 (2005).
[40] W. Chin, F. Piuzzi, J. P. Dognon, I. Dimicoli, and M. Mons, J. Chem. Phys. **123**, 84301 (2005).
[41] I. Hunig, K. A. Seefeld, and K. Kleinermanns, Chem. Phys. Lett. **369**, 173 (2003).
[42] V. A. Shubert and T. S. Zwier, J. Phys. Chem. A **111**, 13283 (2007).
[43] M. Karas, D. Bachmann, U. Bahr, and F. Hillenkamp, Int. J. Mass Spectrom. **78**, 53 (1987).
[44] M. Karas and F. Hillenkamp, Anal. Chem. **60**, 2299 (1988).
[45] J. B. Fenn, M. Mann, C. K. Meng, S. F. Wong, and C. M. Whitehouse, Mass Spectrom. Rev. **9**, 37 (1990).
[46] J. B. Fenn, M. Mann, C. K. Meng, S. F. Wong, and C. M. Whitehouse, Science **246**, 64 (1989).
[47] G. Vonhelden, T. Wyttenbach, and M. T. Bowers, Int. J. Mass Spectrom. **146**, 349 (1995).
[48] T. Wyttenbach, G. vonHelden, and M. T. Bowers, J. Am. Chem. Soc. **118**, 8355 (1996).
[49] L. S. Wang and X. B. Wang, J. Phys. Chem. A **104**, 1978 (2000).
[50] S. E. Rodriguez-Cruz, J. T. Khoury, and J. H. Parks, J. Am. Soc. Mass Spectr. **12**, 716 (2001).
[51] A. T. Iavarone and J. H. Parks, J. Am. Chem. Soc. **127**, 8606 (2005).
[52] L. H. Andersen, A. Lapierre, S. B. Nielsen, I. B. Nielsen, S. U. Pedersen, U. V. Pedersen, and S. Tomita, Eur. Phys. J. D **20**, 597 (2002).
[53] S. B. Nielsen, A. Lapierre, J. U. Andersen, U. V. Pedersen, S. Tomita, and L. H. Andersen, Phys. Rev. Lett. **87**, 228102 (2001).
[54] H. B. Oh, C. Lin, H. Y. Hwang, H. L. Zhai, K. Breuker, V. Zabrouskov, B. K. Carpenter, and F. W. McLafferty, J. Am. Chem. Soc. **127**, 4076 (2005).

[55] H. Oh, K. Breuker, S. K. Sze, Y. Ge, B. K. Carpenter, and F. W. McLafferty, P. Natl Acad. Sci. USA **99**, 15863 (2002).
[56] J. Oomens, N. Polfer, D. T. Moore, L. van der Meer, A. G. Marshall, J. R. Eyler, G. Meijer, and G. von Helden, Phys. Chem. Chem. Phys. **7**, 1345 (2005).
[57] A. Kamariotis, O. V. Boyarkin, S. R. Mercier, R. D. Beck, M. F. Bush, E. R. Williams, and T. R. Rizzo, J. Am. Chem. Soc. **128**, 905 (2006).
[58] R. A. Jockusch, A. S. Lemoff, and E. R. Williams, J. Phys. Chem. A **105**, 10929 (2001).
[59] N. A. Macleod and J. P. Simons, Mol. Phys. **104**, 3317 (2006).
[60] T. D. Vaden, T. de Boer, J. P. Simons, and L. C. Snoek, Phys. Chem. Chem. Phys. **10**, 1443 (2008).
[61] T. D. Vaden, T. de Boer, J. P. Simons, L. C. Snoek, S. Suhai, and B. Paizs, J. Phys. Chem. A **112**, 4608 (2008).
[62] D. Nolting, C. Marian, and R. Weinkauf, Phys. Chem. Chem. Phys. **6**, 2633 (2004).
[63] H. Kang, C. Jouvet, C. Dedonder-Lardeux, S. Martrenchard, G. Gregoire, C. Desfrancois, J. P. Schermann, M. Barat, and J. A. Fayeton, Phys. Chem. Chem. Phys. **7**, 394 (2005).
[64] S. R. Mercier, O. V. Boyarkin, A. Kamariotis, M. Guglielmi, I. Tavernelli, M. Cascella, U. Rothlisberger, and T. R. Rizzo, J. Am. Chem. Soc. **128**, 16938 (2006).
[65] J. A. Stearns, O. V. Boyarkin, and T. R. Rizzo, J. Am. Chem. Soc. **129**, 13820 (2007).
[66] J. A. Stearns, M. Guidi, O. V. Boyarkin, and T. R. Rizzo, J. Chem. Phys. **127**, 154322 (2007).
[67] J. A. Stearns, S. Mercier, C. Seaiby, M. Guidi, O. V. Boyarkin, and T. R. Rizzo, J. Am. Chem. Soc. **129**, 11814 (2007).
[68] S. Mercier, Ph.D. thesis, Ecole Polytechnique Fédérale de Lausanne, 2008.
[69] J. A. Stearns, C. Seaiby, O. V. Boyarkin, and T. R. Rizzo, Phys. Chem. Chem. Phys. **11**, 125 (2009).
[70] M. Guidi, U. J. Lorenz, G. Papadopoulos, O. V. Boyarkin, and T. R. Rizzo, J. Phys. Chem. A **113**, 797 (2009).
[71] Z. Y. Nie, Y. K. Tzeng, H. C. Chang, C. C. Chiu, C. Y. Chang, C. M. Chang, and M. H. Tao, Angew. Chem. Int. Edit. **45**, 8131 (2006).
[72] S. A. Trauger, T. Junker, and G. Siuzdak, *Modern Mass Spectrometry* (Springer-Verlag Berlin, Berlin, 2003), Vol. 225, p. 265.
[73] J. J. Thomas, R. Bakhtiar, and G. Siuzdak, Accounts Chem. Res. **33**, 179 (2000).
[74] D. Gerlich, Adv. Chem. Phys. **82**, 1 (1992).
[75] D. Gerlich and S. Horning, Chem. Rev. **92**, 1509 (1992).
[76] D. Gerlich, Phys. Scripta **T 59**, 256 (1995).
[77] W. D. Cornell, P. Cieplak, C. I. Bayly, I. R. Gould, K. W. Merz, D. M. Ferguson, D. C. Spellmeyer, T. Fox, J. W. Caldwell, and P. A. Kollman, J. Am. Chem. Soc. **117**, 5179 (1995).
[78] MacroModel, version 9.1 (Schrödinger, LLC, New York, 2005).
[79] M. J. Frisch, G. W. Trucks, H. B. Schlegel, G. E. Scuseria, M. A. Robb, J. R. Cheeseman, J. J. A. Montgomery, T. Vreven, K. N. Kudin, J. C. Burant, J. M. Millam, S. S. Iyengar, J. Tomasi, V. Barone, B. Mennucci, M. Cossi, G. Scalmani, N. Rega, G. A. Petersson, H. Nakatsuji, M. Hada, M. Ehara, K. Toyota, R. Fukuda, J. Hasegawa, M. Ishida, T. Nakajima, Y. Honda, O. Kitao, H. Nakai, M. Klene, X. Li, J. E. Knox, H. P. Hratchian, J. B. Cross, V. Bakken, C. Adamo, J. Jaramillo, R. Gomperts, R. E. Stratmann, O. Yazyev, A. J. Austin, R. Cammi, C. Pomelli, J. W. Ochterski, P. Y. Ayala, K. Morokuma, G. A. Voth, P. Salvador, J. J. Dannenberg, V. G. Zakrzewski, S. Dapprich, A. D. Daniels, M. C. Strain, O. Farkas, D. K. Malick, A. D. Rabuck, K. Raghavachari, J. B. Foresman, J. V. Ortiz, Q. Cui, A. G. Baboul, S. Clifford, J. Cioslowski, B. B. Stefanov, G. Liu, A. Liashenko, P. Piskorz, I. Komaromi, R. L. Martin, D. J. Fox, T. Keith, M. A. Al-Laham, C. Y. Peng, A. Nanayakkara, M. Challacombe, P. M. W. Gill, B. Johnson, W. Chen, M. W. Wong, C. Gonzalez, and J.A. Pople, Gaussian 03, Revision D.01 (Gaussian, Inc., Pittsburgh PA, 2004).
[80] A. D. Becke, J. Chem. Phys. **98**, 5648 (1993).

[81] P. C. Hariharan and J. A. Pople, Theoretica Chimica Acta **28**, 213 (1973).
[82] A. Lindinger, J. P. Toennies, and A. F. Vilesov, J. Chem. Phys. **110**, 1429 (1999).
[83] L. I. Grace, R. Cohen, T. M. Dunn, D. M. Lubman, and M. S. de Vries, J. Mol. Spectrosc. **215**, 204 (2002).
[84] K. T. Lee, J. Sung, K. J. Lee, Y. D. Park, and S. K. Kim, Angew. Chem. Int. Edit. **41**, 4114 (2002).
[85] C. R. Cantor and P. R. Schimmel, *Techniques for the study of biological structure and function* (W. H. Freeman, San Francisco, 1980).
[86] O. V. Boyarkin, S. R. Mercier, A. Kamariotis, and T. R. Rizzo, J. Am. Chem. Soc. **128**, 2816 (2006).
[87] F. O. Talbot, T. Tabarin, R. Antoine, M. Broyer, and P. Dugourd, J. Chem. Phys. **122**, 061101 (2005).
[88] N. M. Lakin, R. V. Olkhov, and O. Dopfer, Faraday Discuss. **118**, 455 (2001).
[89] H. Kang, C. Dedonder-Lardeux, C. Jouvet, S. Martrenchard, G. Gregoire, C. Desfrancois, J. P. Schermann, M. Barat, and J. A. Fayeton, Phys. Chem. Chem. Phys. **6**, 2628 (2004).
[90] H. Kang, C. Dedonder-Lardeux, C. Jouvet, G. Gregoire, C. Desfrancois, J. P. Schermann, M. Barat, and J. A. Fayeton, J. Phys. Chem. A **109**, 2417 (2005).
[91] H. Kang, C. Jouvet, C. Dedonder-Lardeux, S. Martrenchard, C. Charriere, G. Gregoire, C. Desfrancois, J. P. Schermann, M. Barat, and J. A. Fayeton, J. Chem. Phys. **122**, 084307 (2005).
[92] W. H. Qiu, L. Y. Zhang, O. Okobiah, Y. Yang, L. J. Wang, D. P. Zhong, and A. H. Zewail, J. Phys. Chem. B **110**, 10540 (2006).
[93] J. A. Stearns, O. V. Boyarkin, and T. R. Rizzo, Chimia **62**, 240 (2008).
[94] R. R. Hudgins, M. A. Ratner, and M. F. Jarrold, J. Am. Chem. Soc. **120**, 12974 (1998).
[95] R. R. Hudgins and M. F. Jarrold, J. Am. Chem. Soc. **121**, 3494 (1999).
[96] R. D. F. Settle and T. R. Rizzo, J. Chem. Phys. **97**, 2823 (1992).
[97] O. V. Boyarkin, R. D. F. Settle, and T. R. Rizzo, Ber. Bunseges. Phys. Chem. **99**, 504 (1995).
[98] O. V. Boyarkin, L. Lubich, R. D. F. Settle, D. S. Perry, and T. R. Rizzo, J. Chem. Phys. **107**, 8409 (1997).
[99] B. Lucas, M. Barat, J. A. Fayeton, C. Jouvet, P. Carcabal, and G. Gregoire, Chem. Phys. **347**, 324 (2008).
[100] B. Lucas, M. Barat, J. A. Fayeton, M. Perot, C. Jouvet, G. Gregoire, and S. B. Nielsen, J. Chem. Phys. **128**, 64302 (2008).
[101] G. Gregoire, B. Lucas, M. Barat, J. A. Fayeton, C. Dedonder-Lardeux, and C. Jouvet, Eur. Phys. J. D **51**, 109 (2009).
[102] A. Stuchebrukhov, S. Ionov, and V. Letokhov, J. Phys. Chem. **93**, 5357 (1989).
[103] A. A. Makarov, I. Y. Petrova, E. A. Ryabov, and V. S. Letokhov, J. Phys. Chem. A **102**, 1438 (1998).
[104] J. D. Chai and M. Head-Gordon, J. Chem. Phys. **128**, 084106 (2008).
[105] T. Benighaus, R. A. DiStasio, R. C. Lochan, J. D. Chai, and M. Head-Gordon, J. Phys. Chem. A **112**, 2702 (2008).
[106] H. Valdes, V. Spiwok, J. Rezac, D. Reha, A. G. Abo-Riziq, M. S. de Vries, and P. Hobza, Chem.- Eur. J. **14**, 4886 (2008).
[107] Y. Zhao and D. G. Truhlar, Theor. Chem. Account **120**, 215 (2007).
[108] Y. Zhao and D. G. Truhlar, J. Chem. Theory Comput. **3**, 289 (2007).
[109] J. Cerny, P. Jurecka, P. Hobza, and H. Valdes, J. Phys. Chem. A **111**, 1146 (2007).
[110] F. Weigend, M. Haser, H. Patzelt, and R. Ahlrichs, Chem. Phys. Lett. **294**, 143 (1998).